Distribution Agreement

In presenting this thesis or dissertation as a partial fulfillment of the requirements for an advanced degree from Emory University, I hereby grant to Emory University and its agents the non-exclusive license to archive, make accessible, and display my thesis or dissertation in whole or in part in all forms of media, now or hereafter known, including display on the world wide web. I understand that I may select some access restrictions as part of the online submission of this thesis or dissertation. I retain all ownership rights to the copyright of the thesis or dissertation. I also retain the right to use in future works (such as articles or books) all or part of this thesis or dissertation.

Signature:

_____ Date: _____

Isaac Karpovsky

Evaluating Efficacy of CD26+ CAR T Cells in an Orthotopic, Immunocompetent Mouse Model of Pancreatic Ductal Adenocarcinoma

By

Isaac Karpovsky

Master of Science

Graduate Division of Biological and Biomedical Sciences

Cancer Biology

Gregory Lesinski, Ph.D.
Advisor

Chrystal Paulos, Ph.D.
Co-Advisor

Sarwish Rafiq, Ph.D.
Committee Member

Accepted:

Kimberly Jacob Arriola, Ph.D., MPH
Dean of the James T. Laney School of Graduate Studies

Date

Evaluating Efficacy of CD26+ CAR T Cells in an Orthotopic, Immunocompetent Mouse Model of Pancreatic Ductal Adenocarcinoma

By

Isaac Karpovsky

B.S., B.A., Emory University, 2022

Advisors:

Gregory Lesinski, Ph.D. And Chrystal Paulos, Ph.D.

An abstract of a thesis submitted to the Faculty of the James T. Laney School of Graduate Studies of Emory University in partial fulfillment of the requirements for the degree of Master of Science in the Graduate Division of Biological and Biomedical Sciences, Cancer Biology, 2023

Abstract

Evaluating Efficacy of CD26+ CAR T Cells in an Orthotopic, Immunocompetent Mouse Model of Pancreatic Ductal Adenocarcinoma

By Isaac Karpovsky

Pancreatic ductal adenocarcinoma (PDAC) is an extremely difficult cancer to treat, with an abysmal 12% 5-year survival rate. At present, chemotherapy confers little benefit, targeted therapies are limited in success, and surgery is considered the only curative approach. Clearly, there is an urgent need to pioneer new treatment strategies against this malignancy. Modern developments in immunotherapy research have produced new treatment options for both hematological and solid tumor malignancies, yet efficacy in PDAC remains low due to roadblocks such as identifying tumor-specific antigen targets, overcoming poor T cell persistence and viability, and improving trafficking of immune cells into the disease site. We hypothesized that enriching chimeric antigen receptor (CAR) T cells with a novel subpopulation of memory T cells characterized by high expression of the CD26 cell surface protein would bolster therapeutic persistence and improve antitumor ability when targeting the mesothelin antigen. We further speculated that treating our CAR T cells with a phosphatidylinositol kinase-3 gamma delta (PI3Kδ/γ) inhibitor *ex vivo* would enhance their stem-like phenotype and improve therapeutic capabilities. Herein, we investigate our orthotopic, immunocompetent mouse model's ability to recapitulate the human PDAC tumor microenvironment (TME) and optimize our ability to produce therapeutic CAR T cells. Next, we conduct *in vivo* trials to test the efficacy of our novel immunotherapy and the utility of PI3Kδ/γ inhibition. Our preclinical studies find that CD4+CD26+ CAR T cells produce a therapeutic response and reduce tumor burden in immunocompetent, PDAC-bearing mice. Although a number of challenges remain, our preclinical studies produce bedrock data for the development of a new CAR T cell-mediated therapeutic approach against pancreatic cancer.

Evaluating Efficacy of CD26+ CAR T Cells in an Orthotopic, Immunocompetent Mouse Model of Pancreatic Ductal Adenocarcinoma

By

Isaac Karpovsky

B.S., B.A., Emory University, 2022

Advisors:

Gregory Lesinski, Ph.D. and Chrystal Paulos, Ph.D.

An abstract of a thesis submitted to the Faculty of the James T. Laney School of Graduate Studies of Emory University in partial fulfillment of the requirements for the degree of Master of Science in the Graduate Division of Biological and Biomedical Sciences, Cancer Biology, 2023

Table of Contents

TABLE OF FIGURES

INTRODUCTION

Pancreatic Ductal Adenocarcinoma and the Oppressive Microenvironment

Pancreatic ductal adenocarcinoma (PDAC) is a deadly malignancy with a 12% overall 5-year survival rate [1]. With limited therapeutic options, surgery remains the only curative approach. Unfortunately, few disease-specific symptoms exist in the early stages of the disease, and therefore over 80% of patients are diagnosed with locally advanced or metastatic disease and do not qualify for surgical resection [2]. At present, PDAC is the third leading cause of cancer-related death in the United States, yet incidence is rising: it is projected to become the second-leading cause of cancer-related death by 2030 [3]. Even among patients diagnosed with localized disease (15% of total diagnoses), the survival rate is still an abysmal 44% [1]. The current standard of care includes cytotoxic chemotherapies such as FOLFIRINOX or gemcitabine, with limited improvements to progression-free or overall survival [4]. Although immunotherapeutic options have become popular in other malignancies, they remain ineffective in PDAC patients [5]. Clearly, there is an urgent need to develop new therapeutic strategies for patients with PDAC.

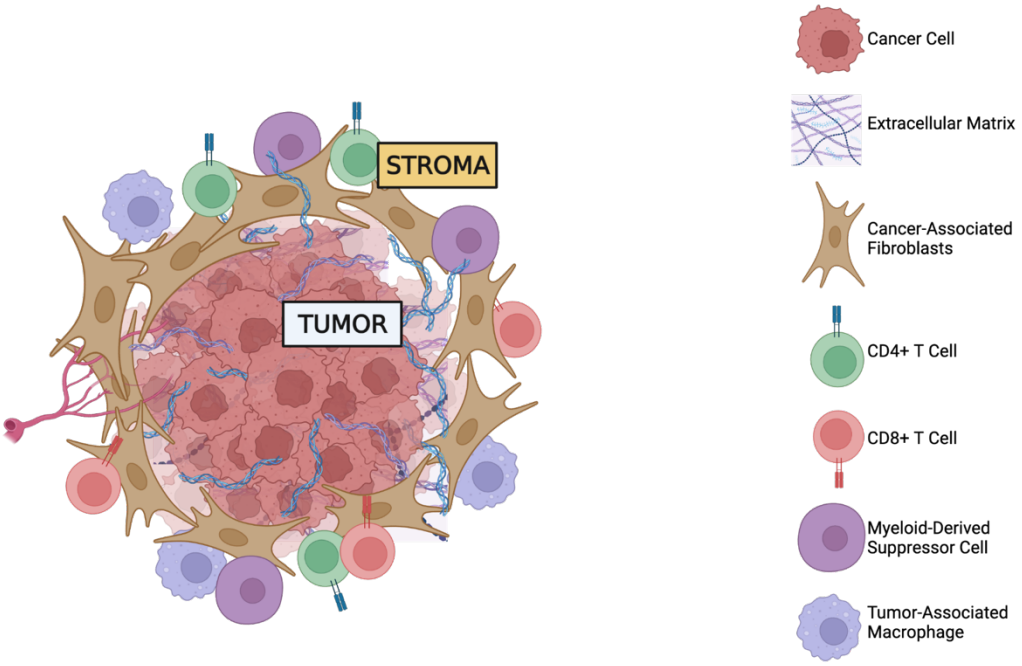

Figure 1: PDAC Tumor Microenvironment.

The PDAC TME consists of various cells and stromal components that interact and crosstalk to create a dense desmoplastic stroma. Cancer-associated fibroblasts (CAFs) produce extracellular matrix proteins such as collagen which create an impenetrable barrier. The stroma is populated with various endothelial and immune populations, including MDSCs and TAMs which contribute to the immunosuppressive phenotype. Lymphocyte infiltration is scarce. Created with BioRender.com

PDAC's refractory nature is strongly related to features of its unique tumor microenvironment (TME); consisting of non-neoplastic cells that crosstalk and interact with PDAC cells to produce a dense, desmoplastic stroma. The TME can account for up to 90% of the tumor by mass, and the grade of desmoplasia in PDAC tumors has been linked to negative survival outcomes and limited efficacy of cytotoxic chemotherapy [6].

There are numerous cell types within the TME that contribute to the cancer's drug resistance, immunologically cold phenotype, and metastatic spread (Figure 1). Briefly, cancer-associated fibroblasts (CAFs) produce extracellular matrix (ECM) constituents such as collagen to support the desmoplastic reaction and increase fibrosis [7]. Desmoplasia, in turn, inhibits drug delivery, limits vascularization, and reduces immune cell infiltration [8]. CAFs are a heterogenous population in both origin and function, however, and also confer an "anchoring" property in PDAC, such that CAF depletion leads to increased metastatic spread and reduced survival [9].

Diverse immune populations exist within the TME, including myeloid-derived suppressor cells (MDSCs), tumor-associated macrophages (TAMs) and various lymphoid lineage cells [10]. TAMs contribute to disease progression and resistance to chemotherapy, while MDSCs adopt a T cell-suppressive phenotype and secrete a large quantity of immunomodulatory soluble factors [11-13]. The most widely studied lymphocytes in PDAC are cytotoxic CD8+ T cells, helper CD4+ T cells, and B cells. T cell populations accounts for less than 1% of total cells in the tumor, a fact that contributes to PDAC's classification as an "immune desert" [14]. Adaptive immunity is further diminished by low mutation burden and lack of tumor-specific antigens, high expression of inhibitory immune checkpoint ligands, and the aforementioned immunosuppressive environment which drastically reduces effector T cell persistence [10].

The abundance of stroma in PDAC tumors and its long reaching effect on treatment outcome has made the TME a sought-after target for therapeutic strategies, including efforts to reprogram stromal components to improve chemotherapy and

immunotherapy efficacy [15, 16]. Overcoming the immunosuppressive TME is an especially relevant challenge for the development of cell therapies against PDAC. A significant current limitation of immunotherapeutic regimens is poor persistence within PDAC tumors, and therefore limited efficacy. Understanding the cellular composition of the TME, its interplay with cancer and the immune system, and its role in treatment outcome is crucial for improving therapeutic options for PDAC.

Immunocompetent, Orthotopic Murine Models of Pancreatic Cancer

To successfully develop immunotherapies for PDAC, one must employ a model system that recapitulates the human malignancy and its abundant desmoplasia. Furthermore, model systems that accurately develop resident immune populations can best portray the immunosuppressive components of the TME, and the impact of these features on therapeutic efficacy. Genetically engineered mouse models (GEMMs) are developed with the same driving mutations as human PDAC patients: specifically, with a G12D mutation in the KRAS oncogene and TP53 knockout. By inducing these genetic mutations, GEMMs develop spontaneous PDAC tumors that follow the same developmental trajectory as human patients. Thus, GEMM tumors are considered the gold standard for modeling tumor composition *in vivo* [17]. Unfortunately, GEMMs are expensive and time-consuming, creating significant drawbacks in their use for large animal studies.

By using immunocompetent, orthotopic tumor mouse models, our studies have the dual-benefit of enabling donor-host immune interactions, as well as tissue site-specific tumor pathology that—as demonstrated within this thesis—accurately recapitulates the TME of a human PDAC patient. While human xenograft models lack a

component immune system and subcutaneous tumors lack site-specific physiology, our orthotopic model produces the best of both worlds without the time commitment and cost associated with GEMMs.

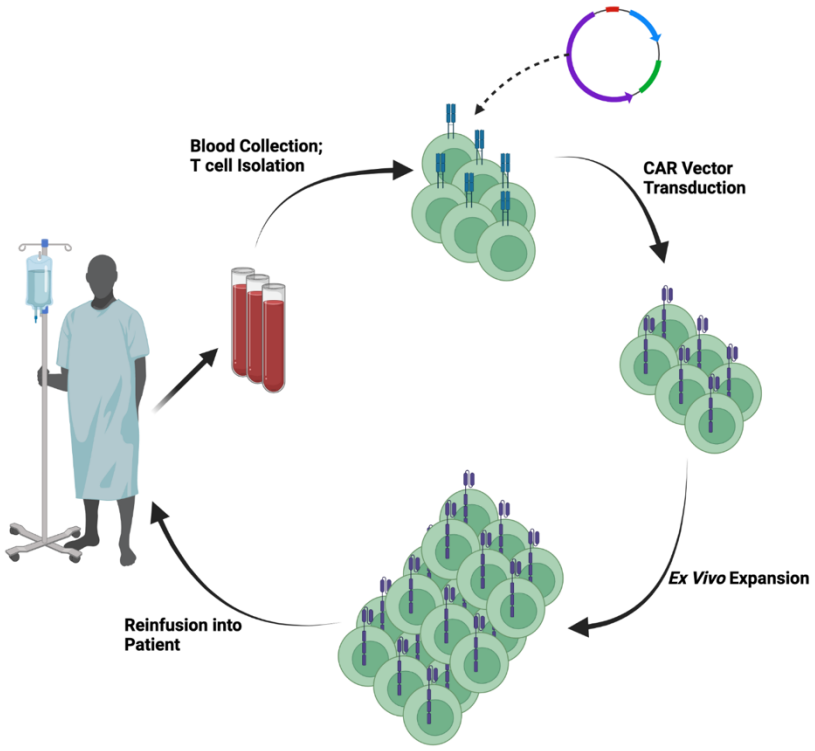

Figure 2: CAR T Cell Development Schema.

T cells are collected and isolated from patient blood samples and genetically modified to express a chimeric antigen receptor that targets a tumor antigen of interest, without relying on MHC presentation. CAR T cells are expanded ex vivo and reinfused into the patient. Created with BioRender.com

Chimeric Antigen Receptor T Cell Therapy: Benefits and Roadblocks

Over the last decade, immunotherapies have transformed the approach to treating several hematological and solid tumor malignancies. In particular, blockade of inhibitory checkpoint receptors on immune cells has become the standard of care

across tumor types including melanoma, renal cell carcinoma, lung cancer and several others [18]. Unfortunately, due to a low mutational burden and the aforementioned hostile TME, effector T cell infiltration into PDAC tumors is minimal, and checkpoint blockade efficacy remains limited [19].

Recently, adoptive cell transfer (ACT) therapy has shown promise in difficult-to-treat and relapsed malignancies, and developments in gene therapy have enabled engineering of tumor-specific T lymphocytes with either chimeric antigen receptors (CAR) T or T cell receptors (TCR). CAR T cells have emerged as a promising treatment option for subsets of hematologic malignancies: there are currently six FDA-approved CAR T cell therapies for leukemia, lymphoma, and myeloma [20]. Although lagging behind in solid tumors, there is robust ongoing research into CAR T cell development with a particular focus on using naïve memory T cells to maintain a long-term antitumor response [21]. Significantly, CD4+ CAR T cells persist in patients for over a decade with sustained cytotoxic function [22]. Although the literature suggests that a 1:1 ratio of CD4 to CD8 T cells confers the optimal therapeutic result, the efficacy of CD4+ CAR T cells alone provides strong evidence for their potential ability to treat PDAC tumors [23].

The composition of a CAR T cell confers certain properties that may overcome the roadblocks involved in treating PDAC, including the immunosuppressive TME, lack of lymphocyte infiltration, and poor persistence. Patient lymphocytes are genetically redirected with a CAR vector to target antigens expressed on the surface of cancer cells, effectively harnessing immunity to target and destroy malignancy (Figure 2). The CAR vector commonly contains a single chain variable fragment (scFv) that confers TCR-specific targeting of extracellular antigens from cell-surface proteins expressed by

tumors, thereby enabling major histocompatibility (MHC)-independent T cell activation. The vector also contains a hinge to overcome steric hinderance and facilitate access to the target antigen as well as a transmembrane domain to anchor the CAR and support its stability and function. Finally, there are typically two intracellular domains: an activation domain most commonly comprised of a CD3ζ-derived immunoreceptor tyrosine-based activation motif, as well as a co-stimulatory domain that optimizes T cell activation and function [24]. CD28-domain and 4-1BB-domain CAR T cells are both FDA approved and are associated with high response rates in patients.

Unfortunately, numerous drawbacks must be addressed before CAR T cell therapy can be used in PDAC. Lack of tumor-specific antigens, poor tumor trafficking capabilities, immunosuppressive signaling within the TME, and short T cell half-lives all pose significant hurdles for achieving effective CAR T cell treatment regimens [24]. To address the foremost limitation, prior research has determined that PDAC cells commonly share an overexpressed antigen called mesothelin: a cell surface protein typically expressed on mesothelial cells at lower levels in cardiac tissue and at elevated amounts on tumors [25].

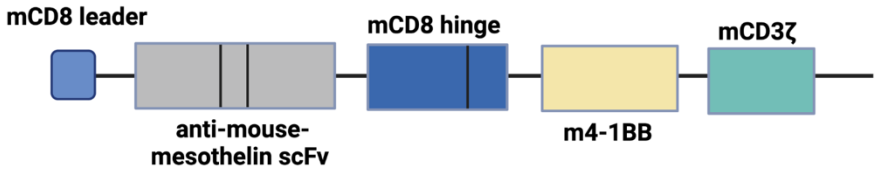

Figure 3: Murine mesoCAR Vector.

Schematic for the mesoCAR vector created using standard gamma retrovirus technology. Synonymous components to the human mesoCAR vector, this version utilizes a mouse-derived scFV for mesothelin as well as mouse-derived intracellular components. Created with BioRender.com based on Watanabe et. al.

To capitalize on this promising antigen, a clinical trial treated patients presenting metastatic PDAC with transiently expressed RNA-encoded CAR T cells targeting mesothelin and found the therapy to be well-tolerated and elicit anti-tumor activity [26]. A subsequent Phase I clinical trial treated patients with lentiviral-encoded mesothelin-specific CAR (mesoCAR) T cells and conferred stable disease in 11/15 patients with PDAC, ovarian carcinoma, or malignant pleural mesothelioma, and only one case of dose-limiting toxicity (grade 4, sepsis) [27]. Unfortunately, efficacy was limited: likely due to previously described roadblocks such as poor infiltration and persistence within the TME. To continue investigating this promising clinical avenue in murine models, our collaborators developed a mouse-specific mesoCAR retroviral vector (Figure 3) [28]. The murine equivalent CAR contains an anti-mouse-mesothelin scFv, as well as the standard CD3ζ TCR signaling domain and 4-1BB costimulatory domain, which supports T cell differentiation into central memory cells with increased mitochondrial biogenesis

and oxidative metabolism [29]. Utilizing this murine mesoCAR vector and our orthotopic PDAC mouse models, we sought out to augment CAR T cell therapy and overcome the current roadblocks for efficacious treatment.

$CD26^{neg}$	$CD26^{int}$	$CD26^{high}$
↑Migratory Capacity ↑Regulatory Properties ↑Sensitivity to Cell-Death ↓Persistence ↓Antitumor activity	↓Migratory Capacity ↑Stemness ↑Persistence ↑Antitumor Activity	↑Migratory Capacity ↑Anti-apoptotic Features ↑Stemness ↑Persistence ↑Polyfunctional Cytokine Release ↑Antitumor Activity

Table One: CD4+ Helper T Cell Subsets by CD26 Expression.

Observations from the Paulos lab have identified three distinct subpopulations of CD4+ helper T cells, as determined by the amount of CD26 expression on their cell-surface. Most importantly, $CD26^{high}$ T cells have anti-apoptotic and stem-like features, long-term persistence in vivo, multifunctional cytokine secretion, and retain a cytotoxic functionality. Taken together, these phenotypes make the subpopulation an ideal candidate for hosting ACT therapies in solid malignancies.

CD26: A Multifunctional Protein of Interest

CD26—also known as dipeptidyl peptidase IV (DPPIV)—is a multifunctional glycoprotein that is well-studied in autoimmune diseases such as diabetes and is

actively being investigated on various cell types in the context of cancer, including CAFs, cancer cells, macrophages, and CD4+ T lymphocytes. On T cells, CD26 is cell-surface co-stimulatory molecule with enzymatic activity and functional properties. Specifically, CD26 can activate antigen-presenting cells, enzymatically cleave chemokines with an X-Pro-motif at the N terminus, bind extracellular matrix proteins such as collagen and fibronectin, and contribute to T cell co-stimulation. [30] CD26+ T cells have been shown to co-secrete numerous cytokines in a Th17-like manner, including IL-17A, IL-22, IFN-γ, and TNFα.

Most importantly, prior published studies identify a subpopulation of T cells with high expression of CD26 (CD26-high) which are characterized by a unique chemokine receptor profile, cytokine production (including cytotoxic granules), a stem memory-like phenotype as measured by elevated lef-1 and β-catenin expression, and robust anti-tumor activity (Table 1) [31]. Notably, these cells demonstrated significant trafficking and tumor-killing abilities when administered as an adoptive cell therapy in NOD scid gamma (NSG) murine models [30]. We speculate that the subpopulation's strong memory characteristics and polyfunctional capabilities will improve their ability to infiltrate and survive within the immunosuppressive TME, and therefore we believe that CD26-high T cells will be ideal hosts for cellular therapeutics in PDAC tumors.

Phosphatidylinositol Kinase-3 δ/γ Inhibition Enhances Therapeutic Function

ACT therapies for PDAC are limited by poor trafficking and migration ability, immunosuppressive conditions within the TME, and poor CAR T cell persistence [32]. In part, therapeutic persistence is likely shortened by a large population of terminally differentiated lymphocytes with limited immunological memory and loss of cytotoxic

functionality [33]. Prior research has demonstrated that the presence of an FDA-approved phosphatidylinositol kinase-3 gamma delta (PI3Kδ/γ) inhibitor (i.e., duvelisib) *ex vivo* can partially inhibit terminal differentiation and increase the proportion of naïve and central memory T cells within the total CAR T cell population. These T cell phenotypes are capable of rapidly differentiating into effector cells with significant antitumor activity, as well as memory cells that improve persistence and long-term response. Furthermore, treating CAR T cells with duvelisib improved the cells' cytokine expression, cytotoxic activity, and expansion abilities *in vivo* [34]. By incorporating duvelisib treatment into the CAR T cell expansion protocol, we aim to further improve the bioenergetics and overall persistence of our novel therapeutic CD26-high CAR T cells.

Scope of Scientific Work

Herein, I aim to assess the efficacy of and conduct foundational pre-clinical studies on CD26-high mesoCAR T cell therapy in relevant models of PDAC. Although mesoCAR T cells are well-tolerated, there are still major roadblocks that must be addressed before their full potential can be leveraged. Due to poor T cell persistence, after entering the blood supply, trafficking to the tumor site, infiltrating the TME, and initiating cytotoxicity, the therapeutic cells often dwindle in number and rapidly lose their functional properties. Data from team show that CD26-high T cells have inherent properties that may improve persistence, migration, and sustain antitumor capabilities.

In this thesis, I address two crucial components for optimizing CAR T therapy for PDAC: the ability of adoptively transferred CD26-high mesoCAR T cells to infiltrate and survive in the immunosuppressive PDAC TME, and their ability to persist and proliferate

within the tumor. I hypothesized that immunocompetent, PDAC-bearing mice administered murine CD26-high mesoCAR T cells will experience significant tumor reduction, better survival outcomes, and enhanced donor cell persistence compared to mice treated with unenriched, CD4+ mesoCAR T cells. I further speculated that use of duvelisib during *ex vivo* mesoCAR T cell expansion would promote a more stem-like phenotype and enhance therapeutic infiltration and persistence.

Additionally, in an effort to optimize the way we develop immunotherapies in murine models, a portion of this thesis is dedicated to assessing the physiological accuracy of distinct orthotopic PDAC models. Herein, I provide data suggesting that our murine models recapitulate the human PDAC TME and accurately portray the role of desmoplasia in immunotherapy infiltration. Ultimately, my scientific goal has been to generate preclinical data that will eventually lead to a first-in-human phase 0/1 clinical trial, thereby improving our options to treat pancreatic cancer.

MATERIALS AND METHODS

Cell Lines and Reagents

Three murine pancreatic cancer cell lines were used throughout this study: KPC-luc, MT5, KP2, as well as MT5 cells expressing luciferase (MT5-luc). KPC-luc cells ($Kras^{LSL\text{-}R270H}$, $p53^{-/-}$, Pdx1-cre) were a gift from Dr. Craig Logsdon, MD Anderson Cancer Center and express an enhanced firefly luciferase construct. Cells were cultured

in DMEM (Gibco) with 10% FBS, 10nM L-glutamine and antibiotics (GiminiBio). MT5 cells ($Kras^{LSL\text{-}G12D}$, $Trp53^{LSL\text{-}R270H}$, Pdx1-cre) were a gift from Dr. David Tuveson at Cold Spring Harbor Laboratory, Cold Spring Harbor, NY and were cultured in RPMI-1640 (Gibco) with 10% FBS, 10 mM L glutamine, and antibiotics. KP2 cells (p48-CRE; LSL-KRas/$Kras^{G12D/wt}$; $p53^{flox/wt}$) were gifted by Dr. David G DeNardo from Department of Medicine, Washington University School of Medicine, St. Louis, MO, USA and were cultured in DMEM:F12 (Gibco) with 10% FBS, 10nM L-glutamine and antibiotics [15].

All experimental T cells were harvested from the spleens of either C57BL/6 or C57BL/6_thy1.1 mice according to the protocol found in appendix I. T cells were cultured in DMEM with 10% FBS and antibodies. Magnetic beads (Dynabeads, Life Technologies) coated with antibodies to CD3 and CD28 were produced according to manufacturer's protocols and administered at a 1:1 bead to T cell ratio. One hundred IU/mL rhIL-2 (NIH repository) were added every 2 days or as needed. Best practices for IL2 concentration, bead-activation, and culture conditions were based on recommendations in the literature [35].

Western Blot

Cell lysates were made by mechanical dissociation followed by suspension in RIPA buffer with 10% PMSF and 10% phosphatase and protease inhibitor cocktail. 20ug of lysate was run on a 10% 10-well, 30ug electrophoresis gel with an anti-mouse-mesothelin antibody (Abcam; ab213174) followed by anti-beta actin antibody for loading control (Abcam; ab8226).

T Cell Transduction

MesoCAR T cells were generated by transducing our CD4+ sorted T cells with a chimeric anti-mesothelin single-chain variable fragment fusion protein containing the T cell receptor signaling domain. Generating the CAR vector has previously been described [36]. The full T cell transduction protocol can be found in appendix I. CAR expression was validated and quantified by using a flow cytometry antibody specific to the murine $F(ab')_2$ fragment (Jackson ImmunoResearch, 115-606-006).

Luciferase Transduction

Luciferase transductions on MT5 and KP2 cell lines were done with GeneCopoeia Lentifect™ lentiviral vectors of firefly luciferase, according to the manufacturer's protocol. Briefly, cells were incubated overnight with target virus suspension at an MOI of 10 in the presence of Polybrene. Transduced products were then selected through a puromycin kill-curve (manufacturer's protocol), followed by a single-cell clonal selection and *in vivo* validation. The complete single-cell selection protocol can be found in appendix I.

In Vivo Studies

All animal studies were conducted under an approved institutional animal care and use committee (IACUC) protocol at Emory University. For orthotopic experiments, 2e5 murine PDAC cells (KPC-luc; MT5-luc) were orthotopically implanted into the tail of the pancreas of 6–8-week-old female C57BL/6 mice (The Jackson Laboratory). A comprehensive protocol for orthotopic surgeries can be found in appendix I. Tumors were grown for 7-10 days and randomized by size via bioluminescent imaging (BLI). Total body irradiation (TBI) was performed with 4Gys of X-ray and occurred on day 7 or 10 post-surgery, and ACT treatment was administered via tail vein injection 24 hours

later. Mice were euthanized if they met IACUC-described criteria for euthanasia prior to study completion. All mice were euthanized by CO_2 asphyxiation followed by cervical dislocation.

Flow Cytometry

Murine tumor tissue, spleens, and blood samples were harvested for immunophenotypic analysis by flow cytometry. Cells were stained and incubated at room temperature in the dark for 10 minutes, washed, and fixed in FACS Buffer containing 4% formalin for flow cytometric analysis on a Cytek Aurora flow cytometer (Cytek). Between 10e4 and 10e6 events collected per sample; data analyzed in FlowJo software (BD). For intracellular stains, cells were first stained for surface markers, then fixed and permeabilized using the eBioscience Staining Buffer, according to manufacturer's established protocols. All cells were stained with Zombie Aqua viability dye to detect live and dead cells. A comprehensive list of antibodies used for flow cytometry panels can be found in appendix II.

Immunohistochemistry (IHC)

Formalin fixed paraffin embedded (FFPE) tumors from *in vivo* experiments were subject to IHC analysis as conducted by Emory's Cancer Tissue Pathology Shared Resource. For quantification, images were analyzed using Qupath software (qupath.github.io): the built-in cell detection algorithm was used to quantify total number of cells within a given area, and threshold detection was used to count the number of marker-positive cells present (CD4, CD8, CK19). [37] For picrosirius red, threshold detection was used to quantify positive area of total tumor tissue area. H&E was used to determine and separate viable tumor tissue from non-neoplastic tissue within FFPE

samples, as noted by black outline on IHC images. A comprehensive list of antibodies used for IHC can be found in appendix II.

Statistical Analysis

Statistical analyses were performed on Prism 9 (GraphPad Software). Data obtained by flow cytometry and IHC were log-transformed prior to analysis to meet model assumptions of normality and homoscedasticity. Outcomes were compared with student's p test or if multiple groups were present via ANOVA, followed by pairwise t test to compare groups for significance. P-values of less than 0.05 were considered significant.

RESULTS

Chapter One: Desmoplasia and Therapeutic Infiltration in Orthotopic Tumor Models

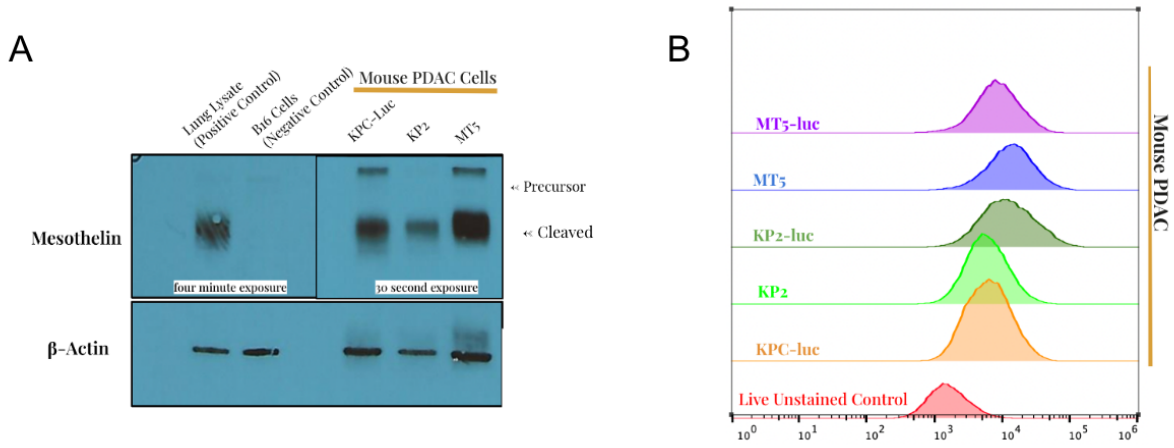

Figure 4: Mesothelin Expression on Murine PDAC.

(A) *Representative blot. Three murine-derived PDAC cell lines (KPC-luc, MT5, KP2) were developed into lysates, stained for mesothelin, and ran through gel electrophoresis to confirm expression.* ***(B)*** *The same three cell lines, as well as luc-expressing derivatives, were stained for flow cytometry along with an unstained control to verify the cell-surface expression of mesothelin. A negative control (B16F10 melanoma cell line) was analyzed but not pictured.*

Mesothelin is Expressed on Mouse-Derived PDAC Cell Lines

We first hypothesized that mouse derived PDAC tumors would express mesothelin: a target for our CAR therapy. To test this idea, we evaluated mesothelin expression on a panel of our murine PDAC cell lines. Mouse lungs were harvested and developed into a lysate as a positive control for western blot, as lungs are known to carry mesothelial cells with mesothelin protein. Our data indicated all three murine cell lines had abundant expression of mesothelin: appearing in both the precursor and cleaved form (Figure 4A). Because CAR T cells are most adept at targeting cell-surface antigens, we further verified mesothelin expression was detectable on the cell surface via flow cytometry, comparing expression to an unstained control (Figure 4B).

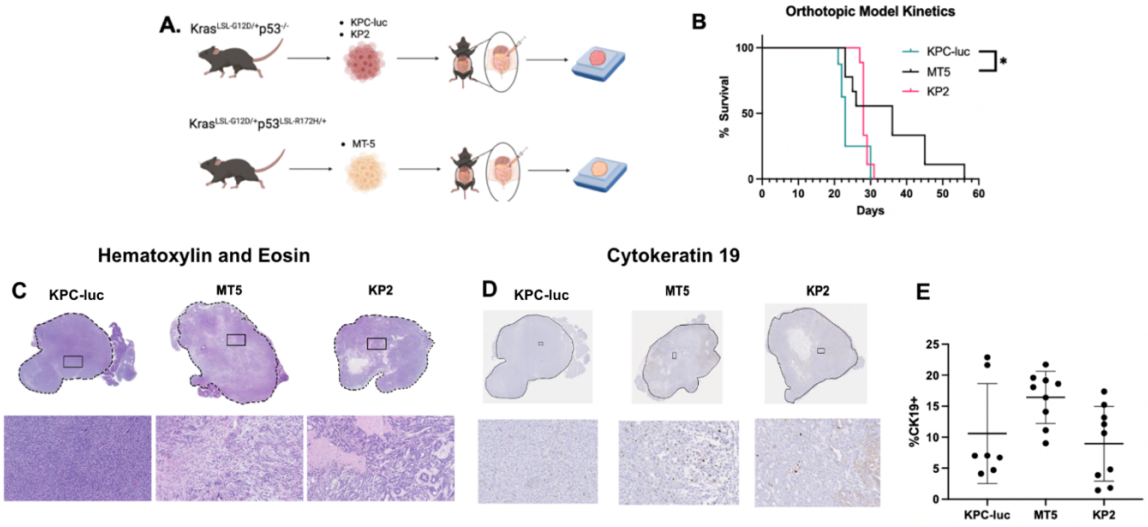

Figure 5: Syngeneic Murine PDAC Cell Lines Differentially Affect Mouse Survival and Tumor Histology.

(A) Cell line development schematic. Each cell line was derived from a KPC GEMM and immortalized for in vitro study. (B) Survival kinetics for PDAC-bearing, immunocompetent mice. Mice were euthanized when IACUC-described criteria were met (n=10 per group). (C) H&E of FFPE tumors derived from each cell line. Topmost image is full-scan, bottom image is 20x magnification. (D) Cytokeratin 19 IHC of FFPE tumors derived from each cell line. Topmost image is full-scan, bottom image is 20x magnification. (E) Quantification of Cytokeratin 19 IHC stain, as measured by % positive cells of total tumor area.

*Black outline denotes area of tissue analyzed. Black squares identify location of magnified images. *Denotes p<0.05*

Syngeneic Models Differentially Affect Mouse Survival and Tumor Histology

In tandem with our preclinical studies on CD26+ CAR T cells, we hypothesized that syngeneic models of PDAC may produce phenotypically different tumors when orthotopically implanted. Although our lab uses immunocompetent mice with orthotopic

PDAC tumors to study novel therapeutic strategies for pancreatic cancer, we have not previously validated whether the tumors recapitulate the degree of desmoplastic stroma that is often observed in human PDAC patients. We used three murine cell lines for our orthotopic surgeries: KPC-luc, MT5, and KP2, all derived from KPC GEMMs and immortalized for *in vitro* and *in vivo* use (Figure 5A). Upon characterizing these cell lines *in vivo*, we noted differential effects on mouse survival and tumor histology across the three models. Mice with KPC-luc and KP2 tumors had a median survival of 23 and 28 days, respectively, while MT5-bearing mice had a median survival time of 36 days (Figure 5B). Hematoxylin & eosin (H&E) staining revealed observable differences in the histology of KPC-luc tumors compared to MT5 and KP2 (Figure 5C). These data prompted us to hypothesize that there would also be differences in the TME of these orthotopic mouse models.

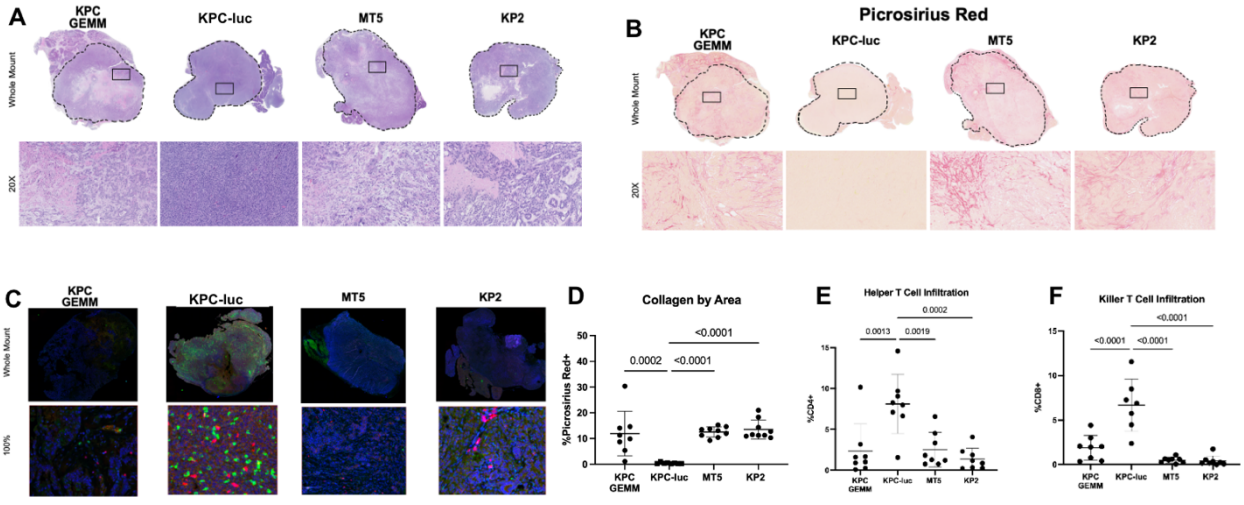

Figure 6: Orthotopic PDAC Tumors Recapitulate the TME of GEMM Tumors.

(A) *H&E of FFPE tumors derived from each cell line and GEMM tumor.* ***(B)*** *Representative image of collagen production, as measured by picrosirius red IHC.* ***(C)*** *Representative image of CD4 and CD8 T cell multiplex IHC. CD4 was stained on opal 690 (red) and CD8 was stained on opal 520 (green).* ***(D)*** *Quantification of stromal fibrosis as measured by picrosirius red positive region of total tumor area.* ***(E)*** *Quantification of CD4+ T cell infiltration, as measured by percent CD4 positive cells out of total cell count in tumor.* ***(F)*** *Quantification of CD8+ T cell infiltration.*

Topmost image is full-scan, bottom image is 20x magnification. Black outline denotes area of tissue analyzed. Black squares identify magnified images.

Orthotopic PDAC Tumors Recapitulate the TME of GEMM Tumors

To address our hypothesis that orthotopic implantation of each cell line produced distinct stromal features, we used immunohistochemistry (IHC) to characterize and quantify various components of the microenvironment. These included histologic analysis via H&E staining, collagen production (picrosirius red), myofibroblast populations (alphaSMA), and T lymphocyte infiltration (CD4 and CD8). A full list of antibodies is in appendix II. We stained orthotopic tumors as well as late-stage KPC GEMM-derived ($Kras^{LSL\text{-}R270H}$, $p53^{-/-}$, Pdx1-cre) tumors that had been previously formalin fixed and paraffin embedded (FFPE). We compared orthotopic tumors to GEMMs because the latter are considered a gold standard for recapitulating the TME of human PDAC patients [38].

Quantifying the stromal components indicated that MT5 and KP2 orthotopic tumors accurately recapitulate the stromal features of the KPC GEMM-derived tumors (Figure 6B, D). Orthotopic KPC-luc tumors, on the other hand, contained significantly

less stroma than GEMM tumors, as measured by collagen production. Furthermore, we observed a strong negative relationship between the amount of desmoplasia and the amount of lymphocyte infiltrates detected in the TME (Figure 6C, E-F). Given the variability in stromal components and lymphocyte infiltration among orthotopic models, we further questioned whether immunotherapy infiltration would be mechanistically affected by grade of desmoplasia when genetic properties are consistent among models.

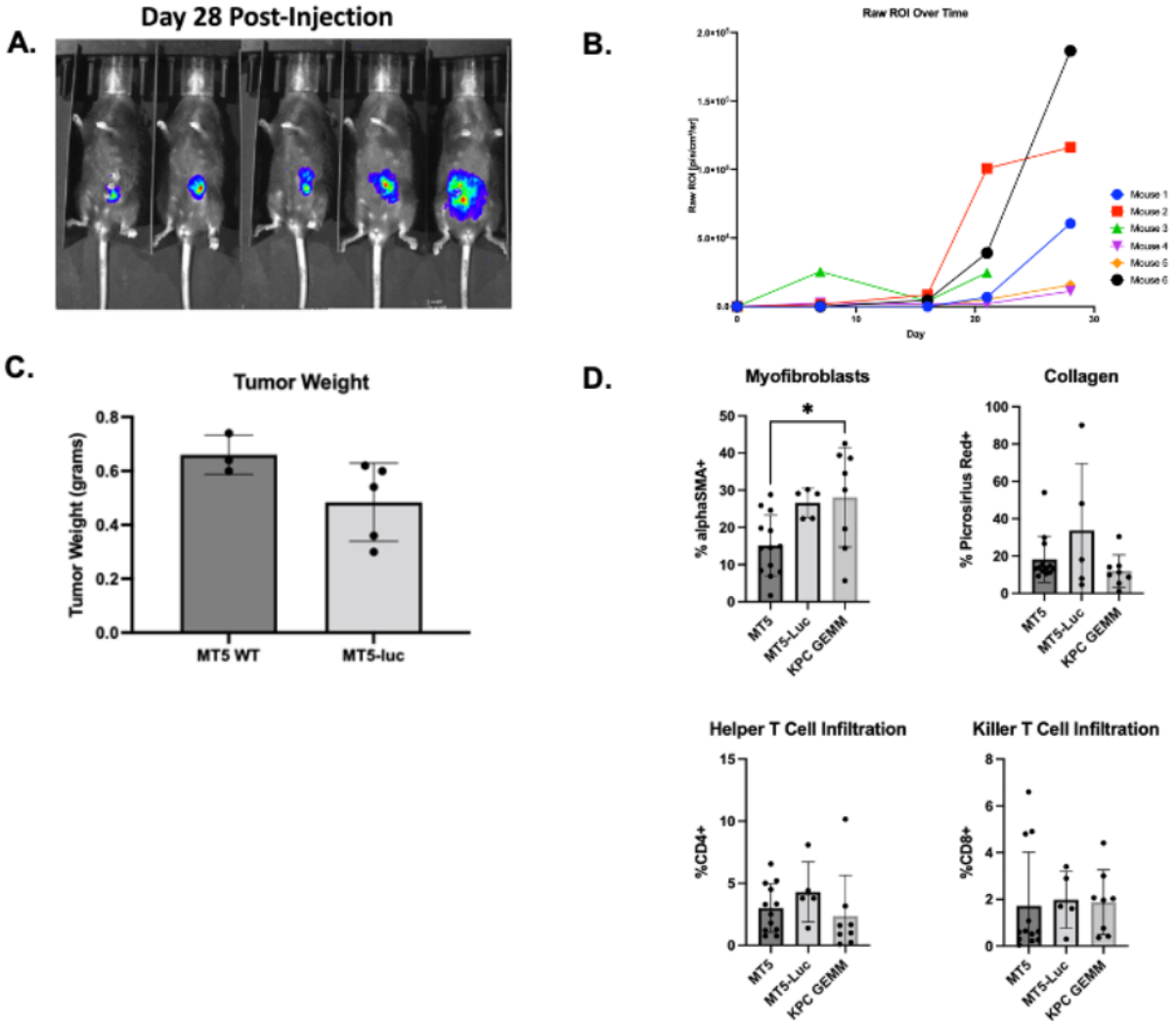

Figure 7: MT5-luc Cells Do Not Undergo Phenotypic Changes *in vivo.*

(A) *Luciferase signaling and absence of host rejection was confirmed via BLI for 28 days.* ***(B)*** *Tumor burden grew consistently as measured by average radiance per region of interest (ROI) without signs of rejection or signal loss.* ***(C)*** *Final tumor weight after 28 days did not vary significantly between MT-5-luc and MT-5 tumor-bearing mice.* ***(D)*** *Quantification of myofibroblast populations, desmoplastic stroma, and T lymphocyte infiltration was determined by IHC and quantified to verify no phenotypic changes have occurred as a result of luciferase transduction. *Denotes p<0.05*

Desmoplastic Stroma Obstructs CAR T Cell Infiltration into the TME

We posited that the degree of desmoplastic stroma would be associated with altered infiltration of adoptively transferred CAR T cells. To address this, we used orthotopic tumor models with murine PDAC cell lines that harbor different propensities for generating collagen-rich tumors. To further improve longitudinal imaging and parity among models, we stably introduced luciferase into the MT5 cell line, so that both KPC and MT5 cell lines could be imaged via BLI. We developed single-cell colonies of MT5-luc to select for pure clonal populations that expressed high levels of luciferase but did not elicit an immune response (protocol can be found in appendix I). We then verified that the resulting cell line experienced no phenotypic changes *in vivo* (Figure 7).

Following cell implantation into the pancreas, tumor growth was verified via BLI after 10 days and mice were lymphodepleted via TBI. We treated all mice with generic, congenic CD3+ mesoCAR T cells for seven days (Figure 8A). The development of mesoCAR T cells is further described in chapter two. Tumors were harvested and split equally between FFPE for IHC and dissociation for tumor infiltrating lymphocyte (TIL) analysis by flow cytometry. Blood was also stained and analyzed by flow cytometry. These data showed significantly less CAR T cell infiltration in stroma-rich MT5-luc tumors, although circulation of therapeutic cells in the blood remained consistent among groups (Figure 8B-E). We further validated the presence of donor CAR T cells in the tumor via IHC staining for thy1.1, the congenic marker found only on the donor T cells (Figure 8F). This experiment contributes novel data in support of an inverse relationship between desmoplasia and T cell infiltration.

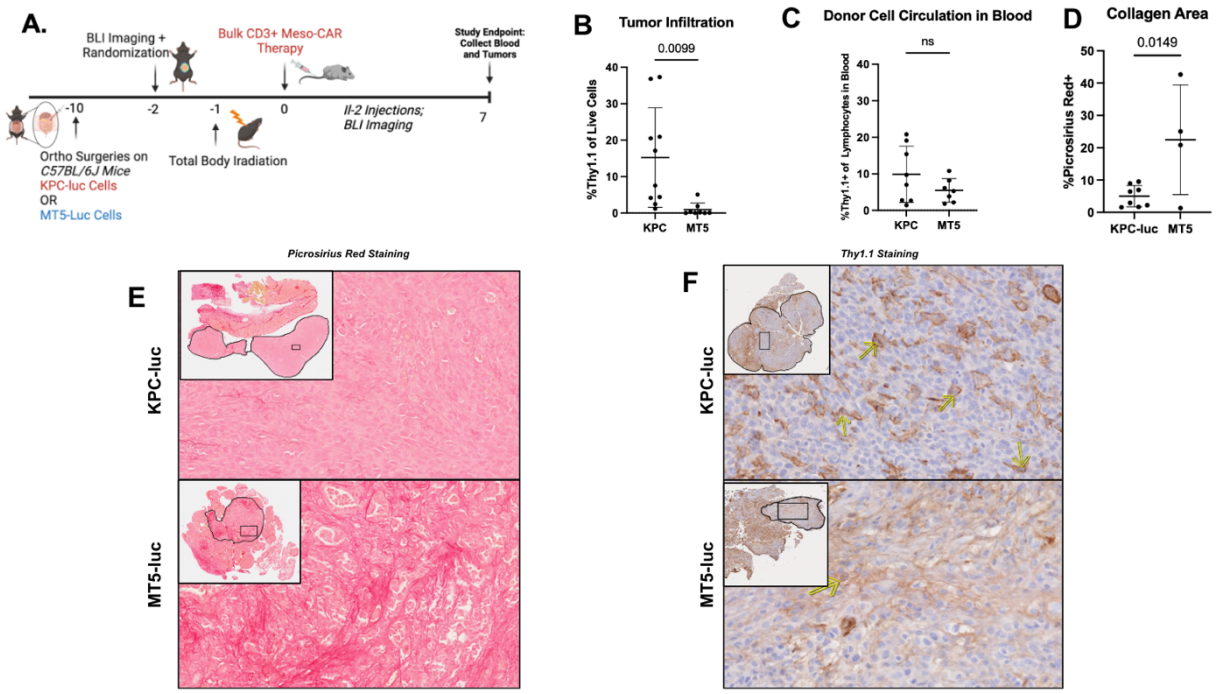

Figure 8: Desmoplastic Stroma Obstructs CAR T Cell Infiltration into the TME. ***(A)*** *Study schematic. Tumors were grown for 10 days before commencing CD3+ mesoCAR T cell treatment for 7 days. Tumors were harvested and split in half for FFPE or dissociation for flow cytometry.* ***(B)*** *Quantification of tumor infiltrating CAR T cells, as measured by thy1.1+ cells of total live cells in tumor sample.* ***(C)*** *Quantification of circulating donor CAR T cells in blood, as measured by proportion of thy1.1+ cells of total lymphocytes in blood samples.* ***(D)*** *Quantification of picrosirius red IHC, as measured by % positive area of total tumor area. Black outline denotes area of tissue analyzed.* ***(E)*** *IHC representative image of tumors stained for picrosirius red as marker for collagen production.* ***(F)*** *IHC representative images of thy1.1+ stain.*

Black outline denotes area of tissue analyzed. Black rectangle locates 40x representative image. Magnified representative images contain yellow arrows pointing towards true-strained infiltrating lymphocytes.

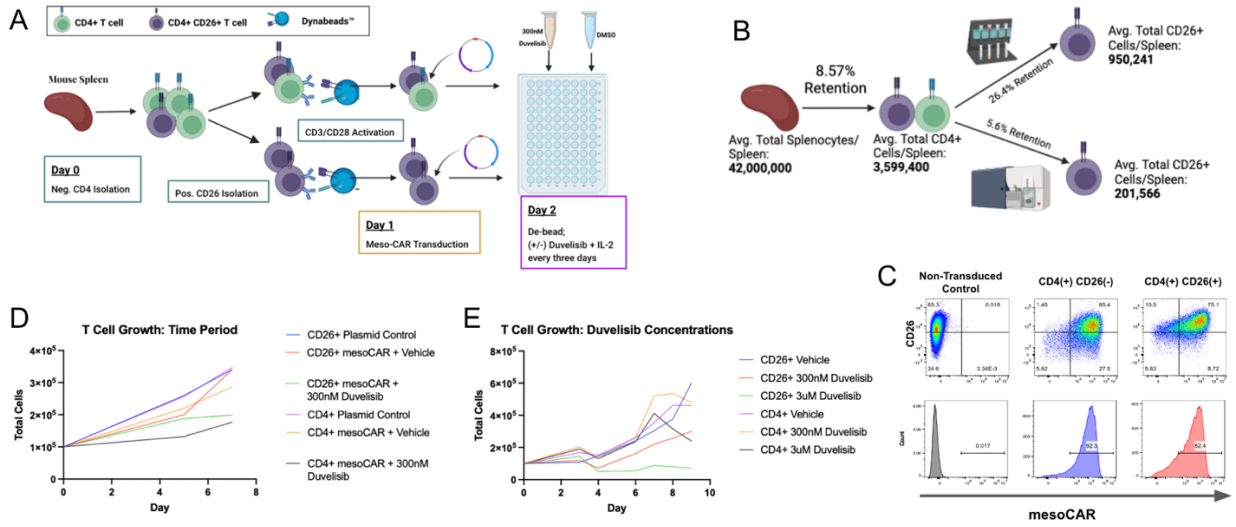

Figure 9: Optimal CAR T Cell Development Protocol.

(A) *Methods schematic; harvests and incubations were done according to previously published practices. CD26+ T cell isolation strategy, duvelisib concentration, and incubation periods were experimentally determined.* ***(B)*** *Harvest and isolation efficiency: an important metric for determining the quantity of spleens one must harvest to complete a preclinical trial.* ***(C)*** *Transduction efficiency for our CD26-low and CD26-high mesoCAR T cells. Because transduction efficiency consistently turned out above 70%, there was no need to further optimize.* ***(D)*** *T cell growth in vitro, groups treated with either vehicle, 300nM, or 3uM of duvelisib to determine optimal drug concentration.* ***(E)*** *T cell growth in vitro. Multiple iterations of the experiment determined that five days was an optimal period for T cell expansion.*

Chapter Two: CD26 mesoCAR Development and *in vitro* Characterization

Optimized CAR T Cell Product Development

As we developed our CAR T cell product, we speculated that certain conditions during production would influence our T cell yield and quality, therefore improving our experimental capabilities. Our goal was to generate cells at a quantity sufficient to administer 1e6 – 1.5e6 therapeutic CAR T cells per animal. Congenic T cells were harvested from spleens, expanded, and transduced according to the protocol described in methods (Figure 9A). On average, CD4+ T cells accounted for 9% of total lymphocytes per mouse spleen when negatively selected with Dynabeads. Of this CD4+ population, positive selection via magnetic beads yielded 26% CD26-high T cells. In an effort to improve cell quality, we explored use of fluorescent-activated cell sorting (FACS). Further described in chapter three, this method reduced the yield of CD26-high T cells to 5.6% of all CD4+ T cells (Figure 9B). Our transduction efficiency remained high throughout the course of the project: consistently yielding above 70% transduced cells (Figure 9C).

Initially, *in vitro* expansion occurred over a 7-day period, but multiple iterations of the experiment produced a cell crash or plateau after day 5, leading us to shorten our incubation period to five days. An additional group of T lymphocytes were concurrently transduced with a plasmid control to determine that the mesoCAR vector did not interfere with T cell growth and proliferation (Figure 9E).

Previous published studies used duvelisib during *ex vivo* expansion of T cells at either 300nM or 3μM concentrations. To determine the optimal concentration for our project, mesoCAR T cells were expanded in the presence of either concentration or vehicle and phenotypes were analyzed via flow cytometry on day 9. Although no

differences in phenotype of cells treated with 300nM and 3μM were evident, there was a clear difference in cell expansion under the two conditions (Figure 9D). To optimize the quantity of T cell yield, we removed the higher dosage and continued future experiments solely with the 300nM concentration of duvelisib.

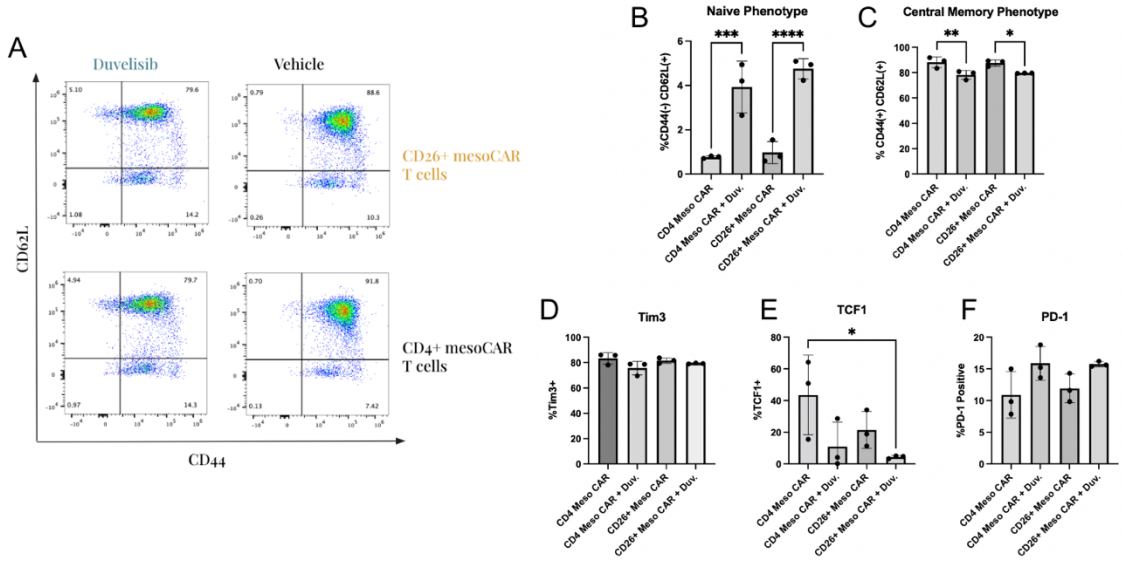

Figure 10: *In Vitro* Effects of Duvelisib on CD26-high CAR T Cell Phenotype.

(A) *Representative Flow Cytometry Schematic demonstrates the changes in central memory and naive T cell phenotype as a product of cell type and duvelisib treatment.* ***(B)*** *Quantification of naive phenotype as measured by CD44(-) CD62L(+) expression.* ***(C)*** *Quantification of central memory phenotype as measured by CD44(+) CD62L(+) expression.* ***(D)*** *Quantification of exhaustion phenotype, as measured by Tim3+ cells.* ***(E)*** *Quantification of stemness, as measured by TCF-1+ cells.* ***(F)*** *Quantification of differentiation, as measured by PD-1+ cells.*

** denotes p<0.05 ** denotes p <0.01 *** denotes p<0.001 **** denotes p<0.0001*

The *in vitro* Effect of Duvelisib on CD26 CAR T Cells

We hypothesized that PI3K inhibition during the expansion of CD26 CAR T cells would prevent their differentiation into a dysfunctional phenotype. To test this concept, we determined how duvelisib would impact the phenotypic properties of CD26-high CAR T cells *in vitro*. Flow cytometric analysis of L-selectin (CD62L) and H-CAM (CD44) was used to classify T cells into a naïve phenotype (CD44-;CD62L+) or a central memory phenotype (CD44+;CD62L+) based on previous literature that has strongly associated the expression of these cell-surface adhesion molecules with memory T cell phenotype [39]. Based on this classification, we observed that duvelisib significantly increases the proportion of CAR T cells with a naïve phenotype, and significantly decreases the proportion of cells with a central memory phenotype (Figure 10A-C).

We also assessed the impact of duvelisib on key T cell characteristics by looking at markers for exhaustion (Tim3), differentiation (PD-1) and stemness (TCF-1). However, in these studies we observed no significant difference when comparing duvelisib-treated cells to vehicle controls, as well as when comparing CD26-high cells to the bulk CD4+ control cells (Figure 10D-F). The lack of stratification based on either of our experimental criteria was the first indication that our method of CD26-high T cell isolation would require further optimization. However, the difference in cell phenotype based on duvelisib treatment supported the continuation with an *in vivo* study. Before proceeding with an ACT therapy trial, we first wanted to determine the accuracy and validity of our orthotopic PDAC mouse models.

Chapter Three: Results and Limitations of Novel CD26-high mesoCAR Therapy

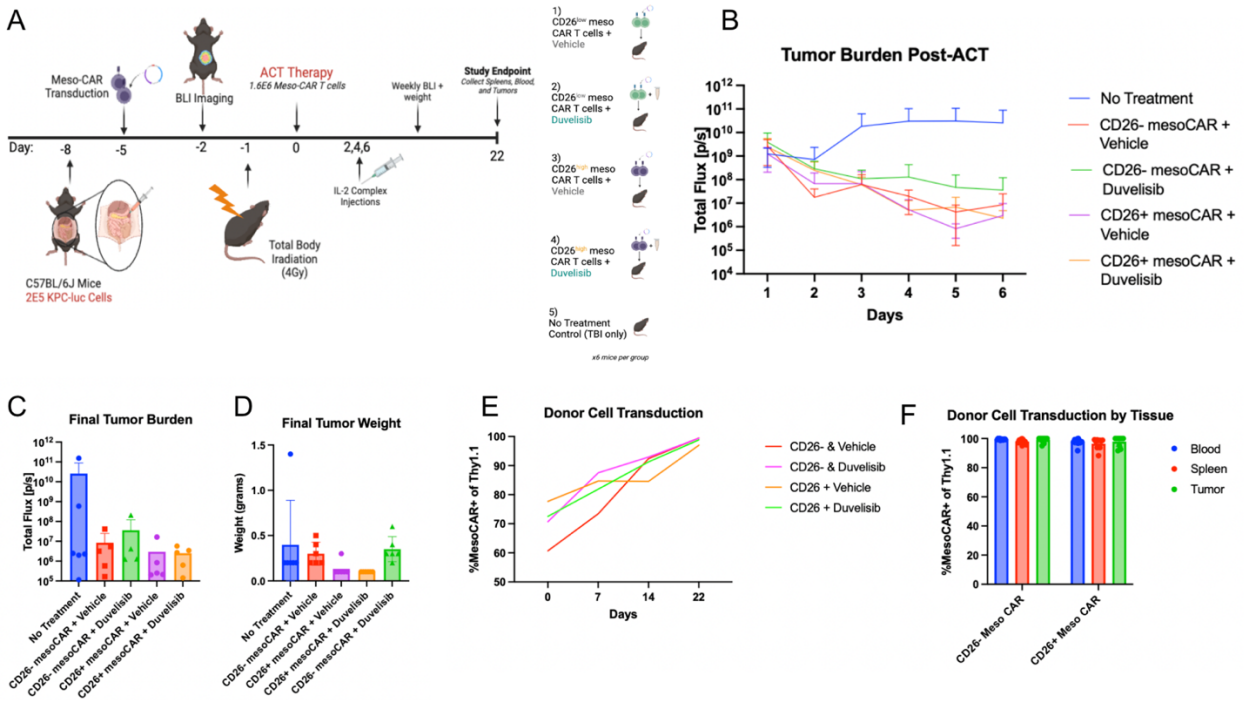

Figure 11: CD26 mesoCAR Therapy Reduces Tumor Burden.

(A) *Study schematic. 22 days of treatment after verifying tumor size and randomizing groups. Each treatment-group mouse received 1.6e6 mesoCAR T cells (n=6 per group).* ***(B)*** *Tumor burden throughout treatment period, as measured by total flux from BLI readings. "CD26- mesoCAR" group encompasses both duvelisib-treated and vehicle-treated groups together; same for "CD26+ mesoCAR" group.* ***(C)*** *Final tumor burden via total flux prior to study endpoint.* ***(D)*** *Final tumor weight as measured upon harvesting tumors.* ***(E)*** *mesoCAR transduction throughout study, as measured by %mesoCAR+ cells of total thy1.1 cell population. Day 0 reading prior to treatment, day 7 and 14 samples drawn via submandibular blood collection.* ***(F)*** *Donor cell transduction at endpoint, as measured by %mesoCAR+ cells of total thy1.1 cell population.*

Pilot Study Shows CD26+ mesoCAR T Cell Efficacy but Fails to Surpass Control

The culmination of this thesis was to address the overarching hypothesis that CD4+CD26+ mesoCAR T cells would have superior antitumor efficacy compared to CD26-low mesoCAR T cells. We further hypothesized that adding duvelisib during *ex*

vivo expansion would improve persistence and foster a more stem-like phenotype prior to *in vivo* administration. An initial pilot study was conducted whereby we implanted immunocompetent mice with KPC-luc tumors and preconditioned the mice with 4Gy of radiation to mimic drug-induced preconditioning in human patients [40]. We confirmed tumors were established via BLI, randomized mice into groups evenly distributed by tumor size and commenced ACT treatment (Figure 11A).

Tumor burden and body weight were recorded for 22 days of treatment, at which point we harvested tumors, blood, and spleens from each mouse to analyze by flow cytometry. Initial results confirmed that administration of CD4+CD26+ mesoCAR T cells reduced tumor burden (Figure 11B-D). Furthermore, we confirmed that only CAR-vector transduced donor T cells were proliferating and surviving. Although ~70% of donor cells initially administered were mesoCAR positive, by end of study 100% of detectable donor cells were positive for the mesoCAR vector (Figure 11E-F). Although these results were promising, they were not significantly different from the treatment control group which received CD26-low mesoCAR T cells.

Donor CAR T cells treated with duvelisib had greater success infiltrating the tumor than vehicle-treated CAR T cells in both CD26-low and CD26-high treatment groups. In both cases, duvelisib-treated cells also persisted in the blood at a greater proportion of total lymphocytes than their vehicle-treated counterparts (Figure 12). Unfortunately, neither duvelisib treatment nor each cell-type had any bearing on T cell stemness, proliferation, or exhaustion. Upon further analysis of the biodistribution data, we noted certain limitations and features of our experimental design that require further

optimization for more definitive future testing. Our next aim was to improve our design and address the model limitations.

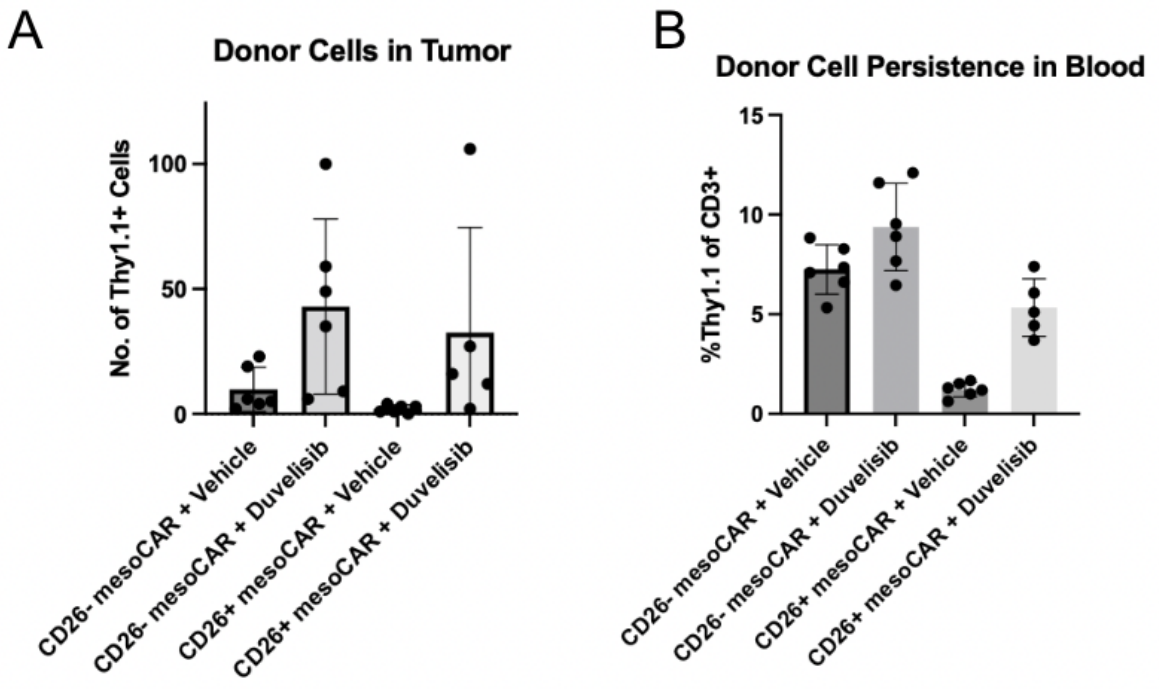

Figure 12: Effect of Duvelisib on mesoCAR T Cells.

(A) *Donor cell count in tumor. Total count of thy1.1+ cells within tumor tissue samples.* ***(B)*** *Donor cell persistence in blood, as measured by %thy1.1+ cells of total CD3+ cells in blood samples.*

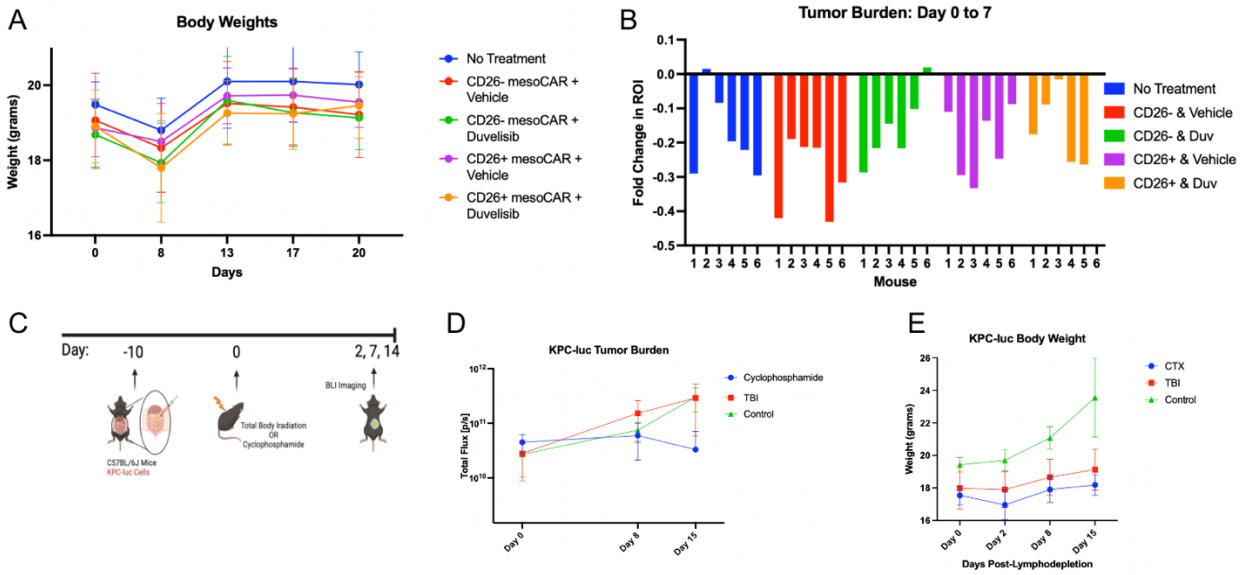

Figure 13: TBI-Induced Toxicity Pilot Study.

(A) *Body weight measurements throughout previously described study.* ***(B)*** *Fold-change in tumor burden from beginning of ACT treatment to day seven of previously described study. Emphasis on drop in tumor burden of no treatment control group.* ***(C)*** *TBI pilot study schematic. PDAC-bearing mice received TBI, cyclophosphamide (CTX), or no treatment to determine the effect of lymphodepletion on tumor growth (n=5 per group).* ***(D)*** *Tumor burden as measured by total flux via BLI.* ***(E)*** *Body weight of mice subject to either TBI, CTX, or no treatment.*

Design Complications and Confounding Factors

There were a number of issues in our initial *in vivo* experimental design that likely confounded the observed results in this pilot study. First, a drop in murine body weight across groups after ACT administration suggested treatment-induced toxicity (Figure 13A). However, all groups—including untreated control—experienced a reduction in tumor burden in the first seven days of treatment (Figure 13B). All groups were subject to TBI, including the no-treatment control, and therefore we conducted a follow-up experiment to assess the effect of TBI on tumor growth. Immunocompetent mice were

surgically induced with orthotopic KPC-luc tumors and after 10 days received TBI, cyclophosphamide (CTX), or were left unhindered (Figure 13C). Ten days was selected as the time point instead of seven days, in an effort to alleviate potential effects of lymphodepletion on cancer growth; the result was minimal loss of tumor burden or body weight following TBI. CTX, however, drastically affected tumor size and was therefore ruled out as a potential substitute (Figure 13D-E).

Second, throughout the study we experienced severe difficulties in our attempts to select for a distinct CD26-high murine T cell population. Initially, we used magnetic beads to positively select for CD26-high T cells, yet, comparing CD26 expression via flow cytometry among murine CD26-high, CD26-low, and CD4+ (unselected) populations yielded an almost negligible difference (Figure 14A). To understand potential root causes of this issue, we compared CD26 expression on human CD4+ T cell populations against mouse CD4+ T cells and found that while human T cells readily stratify into distinct clusters (the aforementioned ‘CD26-low; ‘CD26-int’; ‘CD26-high’ groups), all murine T lymphocytes display similar expression levels of the protein (Figure 14B). We are currently interrogating use of other murine CD26 directed antibodies to identify whether this is an issue with the reagent, or if it reflects the inherent biology of these cells that might differ between mouse and humans. Next, we attempted to isolate our subpopulation of interest via FACS. Although this method was better at segregating murine T cells into CD26-high and CD26-low groups, it came at a drastic loss in total cell yield (Figure 5B). Addressing the discrepancy between human and murine CD26 expression—and our ability to isolate unique populations in the

latter—remains a top priority for the optimization and continuation of this research project.

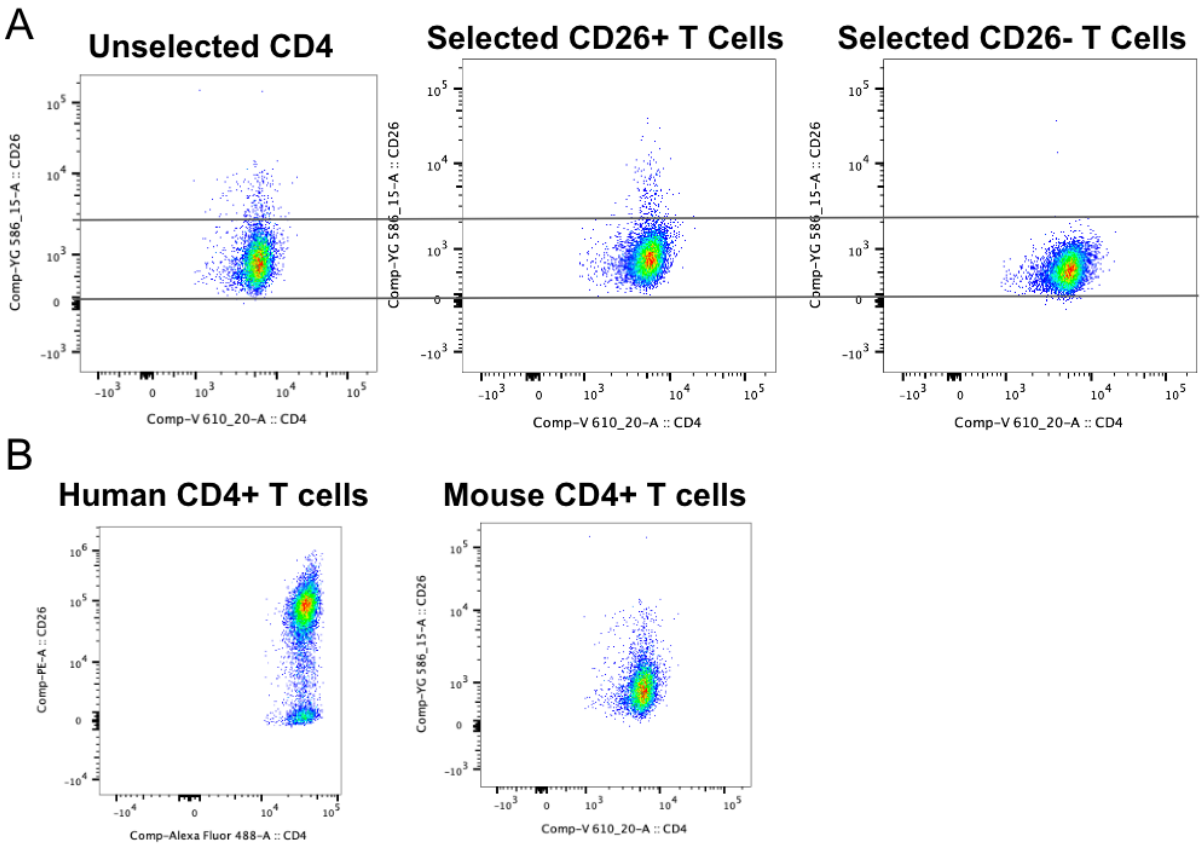

Figure 14: Limitations of Modeling CD26 Expression on Mouse T Cells.

(A) *Unselected CD4+ T cells, positively selected CD26+ T cells, and negatively selected CD26- T cells, demonstrating the poor selection affinity of magnetic beads. Black bars demonstrate the extreme similarity in expression among all three groups.* ***(B)*** *Human and Mouse CD4+ T cells, stratified by CD26 expression demonstrates the clear innate difference between the two species.*

DISCUSSION

In this thesis, I establish a pre-clinical foundation for investigating a novel immunotherapy against PDAC. I describe the development of immune-competent, physiologically accurate mouse models of PDAC and preclinical experiments using mesothelin-specific, CD26-high CAR T cells as an adoptive cell therapy approach. By optimizing our CAR T cell development protocol and verifying our orthotopic murine model's robust histology and cellular composition, I made significant initial strides to address the therapeutic potential of CD26-high CAR T cell therapy. I further attempted to validate whether PI3Kδ/γ inhibition during *ex vivo* T cell expansion bolsters their therapeutic abilities.

Mesothelin is over-expressed in human PDAC tumors and previous studies have validated its potential as a therapeutic target. [25, 27] We were able to verify consistent, cell-surface expression of mesothelin on all of our murine-derived PDAC cell lines via western blot and flow cytometry. Unfortunately, targeting a single antigen in cancer comes with its own challenges, such as antigen escape. Clinical data approximates that 10-25% of patients treated with CD19+ CARs for B cell acute lymphoblastic leukemia experienced relapse with CD19-negative disease [41]. While targeting mesothelin offers a promising avenue for treating PDAC, evidence suggests it will not be sufficient on its own. New research directions are focused on developing CAR T cell technologies to target multiple antigens, thereby reducing the chance of antigen-escape-mediated relapse [42].

The use of immunocompetent, orthotopic mouse models is advantageous for the observation of site-specific tumor pathology, but the accuracy of this model at recapitulating the human PDAC TME has not been previously verified. For our first

research aim, we wanted to validate the physiological accuracy of our orthotopic mouse models. Due to the central role of the TME in PDAC progression and treatment outcomes, accurately modeling the microenvironment is crucial for reducing the disparity between preclinical data and human outcomes. Because GEMMs are developed with the same driving mutations as PDAC, they faithfully recapitulate many histologic, structural, and stromal components of human disease [43, 44]. By quantitatively comparing the composition of our orthotopic tumors to GEMM tumors, we confirmed that the MT5 and KP2 models produce comparable TME features to those found in human PDAC patients. We also demonstrated that KPC-luc tumors contained significantly less stroma and more TILs than the other two models. These findings have important implications for our mouse experiments, as we now know which cell lines to prioritize for future studies. In light of these findings, we developed an MT5-luc cell line to enhance our orthotopic studies and enable tumor monitoring via BLI. When the transduced cells were first implanted *in vivo*, their utility was limited by immunogenicity. To address this issue, we subsequently developed single-cell colonies to select for pure clonal populations that expressed high levels of luciferase but did not elicit an immune response. We then verified that the resulting cell line experienced no phenotypic changes *in vivo*.

Comparing our orthotopic models yielded the following two observations: first, among syngeneic tumor models, there is significant variation in the degree of collagen production, and therefore in the quantity of desmoplastic stroma surrounding the tumors. Second, the amount of stroma surrounding syngeneic tumors negatively correlates with the amount of lymphocyte infiltration into the TME. The unique

differences in our orthotopic models created a new research question: does the degree of desmoplasia associate with reduced infiltration of transferred CAR T cells into PDAC tumors when the genetic properties are synonymous? To test this research aim, we designed a study to investigate the role of collagen in CAR T cell infiltration.

Within the PDAC TME, collagens are the most abundant ECM proteins, and therefore largely contribute to desmoplasia. [45] There is a large body of literature that describes the role of desmoplastic stroma in preventing drug and lymphocyte infiltration into PDAC tumors [10, 14, 46-48]. Yet, there are little data on the relationship between desmoplasia and CAR T cell infiltration. Furthermore, recent studies have argued that collagen within the TME contributes an anchoring role in tumor progression by reducing cancer spread and promoting CD8+ T cell infiltration [49]. Given the uncertainty surrounding these variables, we sought to compare CD3+ CAR T cell infiltrates in syngeneic tumor models with varying amounts of collagen production.

Our results support the notion that access of lymphocytes to PDAC tumors is limited by the cellular components of the PDAC TME [50]. We produced a novel scientific contribution by demonstrating that desmoplastic stroma is associated with reduced infiltration of adoptively transferred T cells in a well characterized murine model of PDAC. By validating the physiological accuracy of KP2- and MT5-derived tumors, we can conclude these models have value for future testing of other targeted and immunotherapy approaches.

To address our second research aim, we explore different strategies for CAR T cell expansion and used flow cytometry to assess the effect of duvelisib on T cell development and phenotype. Our initial protocol was adapted from best practices

established by the Paulos lab [30]. The components of our protocol that matched published results were left unchanged. For instance, administering 10 IU of exogenous IL2— a cytokine that stimulates T cell proliferation— is known to improve *in vitro* CAR T cell expansion [51]. Initially, our preclinical studies included treating mice with IL2 complex *in vivo* as an additional stimulus for T cell proliferation. However, literature suggests that IL2 complex also leads to vigorous proliferation of CD25+CD4+ T-regulatory cells: a specialized subpopulation that suppresses immune response. Because this population would be detrimental to our study goals, assessing the role of IL2 complex *in vivo* is an important future direction for optimizing therapeutic expansion [52]. For subsequent experiments, we removed IL2 complex from our protocol.

Although previous studies have used multiple concentrations of duvelisib during *ex vivo* T cell expansion, we confirmed that 3μM was cytotoxic to our T cell product (Figure 9D). To improve our harvest efficiency, we only treated our cells in the presence of 300nM duvelisib. A highlight of our CAR T cell development protocol has been the retroviral transduction: consistently yielding >70% transduction efficiency. The greatest hurdle we have yet to overcome is optimizing our FACS yield for CD26-high T cells. Our most recent sort produced only 3.15e6 CD26-high T cells from forty congenic mouse spleens. With this existing approach and efficiency, to treat 10 PDAC-bearing mice with one million CD26-high CAR T cells each would require the harvest of 120 congenic mice: a mouse order that would cost nearly $10,000. Clearly, there is a need to improve isolation efficiency or transition away from FACS to another purification strategy or other refined methodologies.

Previously published studies demonstrated the potential benefits of a PI3Kδ/γ inhibitor (duvelisib) as a means to augment T cell functionality. Duvelisib treatment during expansion increases the number of Th17 cells with a central memory phenotype, and decreases regulatory properties (i.e., FoxP3 expression), significantly bolstering the T cells' antitumor capabilities [53]. Follow up studies found that along with priming T cells towards a more central and naïve phenotype, duvelisib treatment also improves CAR T cell expansion, cytotoxicity, and persistence [34]. We reproduced some of these results in our CD26-high CAR T cells, particularly finding that expanding our novel therapy in the presence of duvelisib increases the proportion of naïve T cells, although we also noted a decreased proportion of central memory cells. Our *in vivo* studies suggest that the addition of duvelisib improved CAR T cell infiltration into the tumor as well as improved retention in the blood: ultimately promoting the hypothesis that duvelisib can augment immunotherapy development. We have yet to examine the effect that duvelisib may have on long-term persistence or cytotoxicity.

The primary and final goal of this thesis was to quantify the efficacy and longevity of our murine CD26-high CAR T cells in an immunocompetent mouse model. While our first two research aims established a strong foundation for studying this novel therapy, the third and final aim consisted of preclinical mouse experiments to measure treatment response and donor cell phenotype. Although immune checkpoint blockade has revolutionized treatment options in numerous malignancies, they remain ineffective in PDAC: in part due to low antigenicity and the immunosuppressive TME [54]. Advances in CAR T cell technology offer a promising new avenue for targeting and destroying PDAC without relying on MHC presentation or scarcely available TILs. Phase I clinical

trials targeting human epidermal growth factor receptor 2 (HER-2), CD133, and mesothelin are currently ongoing. Despite these advances, there are still numerous concerns surrounding the CAR T cells' ability to persist long enough within the PDAC TME to mount a sustained clinical response [55]. By enriching our CAR T cell population for memory lymphocytes with a stem-like phenotype—and enhancing their function with PI3Kδ/γ inhibitors—we aim to improve the persistence and efficacy of our novel therapy.

By treating PDAC-bearing mice with CD26-high and CD26-low mesoCAR T cells, we demonstrate decreased tumor burden relative to no-treatment control. By study endpoint, our donor T cells were 100% positive for the mesoCAR vector: a strong indicator that only transduced cells were activating and proliferating. Treating our therapeutic cells with duvelisib improved their tumor-infiltration and slightly increased retention in the blood. These intriguing preliminary data support our hypothesis that as a novel immunotherapy, CD26-high mesoCAR T cells will have potential for efficacy.

Unfortunately, there were components of our hypothesis that we failed to address. Although our CD26-high group reduced tumor burden, there was no significant difference from the CD26-low treatment group. The lack of variability between CD26-high and CD26-low treatments is yet another clue that our method of cell-isolation requires further refinement. Although we attempted to stratify CAR T cell phenotype by cell type and duvelisib treatment, we found no clear patterns in T cell differentiation, exhaustion, or stemness among the four treatment groups in these preliminary studies. Our results show proof-of-concept for the therapeutic potential of CD26-high T cells and offer valuable insights into the characteristics required for an effective and safe therapy.

In this thesis we also address model limitations and potential confounding factors. Lymphodepletion is a commonly used practice in patients prior to receiving CAR T cell therapy, specifically to improve therapeutic expansion and decrease the immunosuppressive cell populations [56]. In this study, we used TBI to mimic the effects of lymphodepletion, but found that subjecting mice to X-rays also reduced tumor growth. Conducting a TBI-focused pilot study helped confirm that preconditioning caused transient toxicity and led us to amend our protocol to allow tumors to develop for 10 days instead of 7 prior to ACT treatment.

Although in human blood samples we can detect a population of T cells with high expression of CD26 protein, the distribution of CD26 on murine T cells likely differs. Our data derived from T cells enriched from spleens and blood of our C57BL/6 mice supports this discordant expression (Figure 14B). As a subset of CD4+ memory T cells, CD26-high lymphocytes may develop as a response to various diseases and vaccinations [31]. Because lab mice are developed in a controlled environment, one theory suggests that a lack of exposure to infectious agents may explain the different distribution of CD26 expression on T cells in mice. The difference in protein expression among species would explain why magnetic beads failed to sort the cell populations and why we failed to see distinct differences among our therapeutic groups. Addressing this model limitation is crucial for any other experiments that wish to utilize murine CD26-expressing T cells, especially in the context of preclinical studies for therapy development.

FUTURE DIRECTIONS

Although this thesis establishes foundational data for testing and developing a CD26-high mesoCAR therapy, there are a number of future directions which will continue to drive this project towards the ultimate goal of safety testing in patients. First, conducting a proliferation assay by co-culturing mesoCAR T cells with mesothelin-expressing PDAC cells (without prior bead activation) will address the therapy's activation and expansion efficiency. Second, any iteration of a cytotoxicity assay will help us determine the cytotoxic function relative to currently available CAR T cell hosts such as CD8+ or CD3+ nonenriched T lymphocytes. Finally, because CD26-high T cells are capable of polyfunctional cytokine expression, collecting murine T cell supernatants for a cytokine analysis will help explore further benefits of this enriched subpopulation.

There are a number of studies necessary to improve the robustness of our model system. One should further validate the results of our tumor infiltration study by conducting an additional experiment with the KP2 cell line and confirm the relationship between desmoplasia and CAR T cell infiltration. A pilot study should also be conducted to determine whether TBI has any effect on cell-surface expression of mesothelin in our murine PDAC tumors.

As previously mentioned, a crucial step for all future studies on this project is to optimize our CD26-high T cell isolation procedure. Given the potential theory that CD26-high expression is missing due to a lack of exposure to infectious agents, one may attempt to immunize mice with a tetanus vaccine to determine if immunological memory leads to the development of our target population [57]. Given what we have learned throughout this thesis about our orthotopic PDAC mouse models and their relative accuracy, it will be important going forward to reproduce our results in one of the more

physiologically accurate PDAC cell lines: MT5, MT5-luc, or KP2. Finally, a significant future experiment will be a survival study to determine whether our novel therapy improves medial murine survival time. The study should include regular blood-draws to monitor CAR T cell circulation and phenotype in the blood, as well as the effect of duvelisib on long-term persistence and T cell function.

REFERENCES

1. *Cancer Facts & Figures.* American Cancer Society, 2023.

2. Ansari, D., A. Gustafsson, and R. Andersson, *Update on the management of pancreatic cancer: Surgery is not enough.* World Journal of Gastroenterology, 2015. **21**(11): p. 3157-3165.

3. Rahib, L., et al., *Projecting Cancer Incidence and Deaths to 2030: The Unexpected Burden of Thyroid, Liver, and Pancreas Cancers in the United States.* Cancer Research, 2014. **74**(11): p. 2913-2921.

4. Grossberg, A.J., et al., *Multidisciplinary standards of care and recent progress in pancreatic ductal adenocarcinoma.* CA: A Cancer Journal for Clinicians, 2020. **70**(5): p. 375-403.

5. Foley, K., et al., *Current progress in immunotherapy for pancreatic cancer.* Cancer Letters, 2016. **381**(1): p. 244-251.

6. Whatcott CJ, P.R., Von Hoff DD, et al. , *Desmoplasia and chemoresistance in pancreatic cancer.. .* Pancreatic Cancer and Tumor Microenvironment. , 2012: p. Chapter 8. Available from: https://www.ncbi.nlm.nih.gov/books/NBK98939/.

7. Pandol, S., et al., *Desmoplasia of Pancreatic Ductal Adenocarcinoma.* Clinical Gastroenterology and Hepatology, 2009. **7**(11): p. S44-S47.

8. Jacobetz, M.A., et al., *Hyaluronan impairs vascular function and drug delivery in a mouse model of pancreatic cancer.* Gut, 2013. **62**(1): p. 112-120.

9. Andrew, et al., *Stromal Elements Act to Restrain, Rather Than Support, Pancreatic Ductal Adenocarcinoma.* Cancer Cell, 2014. **25**(6): p. 735-747.

10. Herting, C.J., I. Karpovsky, and G.B. Lesinski, *The tumor microenvironment in pancreatic ductal adenocarcinoma: current perspectives and future directions.* Cancer and Metastasis Reviews, 2021.

11. Yang, S., Q. Liu, and Q. Liao, *Tumor-Associated Macrophages in Pancreatic Ductal Adenocarcinoma: Origin, Polarization, Function, and Reprogramming.* Front Cell Dev Biol, 2020. **8**: p. 607209.

12. Lauren, et al., *Tumor-Derived Granulocyte-Macrophage Colony-Stimulating Factor Regulates Myeloid Inflammation and T Cell Immunity in Pancreatic Cancer.* Cancer Cell, 2012. **21**(6): p. 822-835.

13. Karakhanova, S., et al., *Characterization of myeloid leukocytes and soluble mediators in pancreatic cancer: importance of myeloid-derived suppressor cells.* OncoImmunology, 2015. **4**(4): p. e998519.

14. Foucher, E.D., et al., *Pancreatic Ductal Adenocarcinoma: A Strong Imbalance of Good and Bad Immunological Cops in the Tumor Microenvironment.* Frontiers in Immunology, 2018. **9**.

15. Zhang, Y., et al., *Heat Shock Protein-90 Inhibition Alters Activation of Pancreatic Stellate Cells and Enhances the Efficacy of PD-1 Blockade in Pancreatic Cancer.* Molecular Cancer Therapeutics, 2021. **20**(1): p. 150-160.

16. Hashimoto, A., et al., *Orchestration of mesenchymal plasticity and immune evasiveness via rewiring of the metabolic program in pancreatic ductal adenocarcinoma.* Front Oncol, 2022. **12**: p. 1005566.

17. Qiu, W. and G.H. Su, *Development of Orthotopic Pancreatic Tumor Mouse Models*. 2013, Humana Press. p. 215-223.

18. Postow, M.A., M.K. Callahan, and J.D. Wolchok, *Immune Checkpoint Blockade in Cancer Therapy.* Journal of Clinical Oncology, 2015. **33**(17): p. 1974-1982.

19. Bian, J. and K. Almhanna, *Pancreatic cancer and immune checkpoint inhibitors—still a long way to go.* Translational Gastroenterology and Hepatology, 2021. **6**: p. 6-6.

20. NCI, N.C.I., *CAR T Cells: Engineering Patients' Immune Cells to Treat Their Cancers.* Cancer.Gov, 2022.

21. Hinrichs, C.S., et al., *Adoptively transferred effector cells derived from naïve rather than central memory CD8 ⁺ T cells mediate superior antitumor immunity.* Proceedings of the National Academy of Sciences, 2009. **106**(41): p. 17469-17474.

22. Flemming, A., *Cytotoxic CD4+ CAR T cells implicated in long-term leukaemia remission.* Nature Reviews Immunology, 2022. **22**(3): p. 146-146.

23. Melenhorst, J.J., et al., *Decade-long leukaemia remissions with persistence of CD4+ CAR T cells.* Nature, 2022. **602**(7897): p. 503-509.

24. Rafiq, S., C.S. Hackett, and R.J. Brentjens, *Engineering strategies to overcome the current roadblocks in CAR T cell therapy.* Nature Reviews Clinical Oncology, 2020. **17**(3): p. 147-167.

25. Pastan, I. and R. Hassan, *Discovery of Mesothelin and Exploiting It as a Target for Immunotherapy.* Cancer Research, 2014. **74**(11): p. 2907-2912.

26. Beatty, G.L., et al., *Activity of Mesothelin-Specific Chimeric Antigen Receptor T Cells Against Pancreatic Carcinoma Metastases in a Phase 1 Trial.* Gastroenterology, 2018. **155**(1): p. 29-32.

27. Haas, A.R., et al., *Phase I Study of Lentiviral-Transduced Chimeric Antigen Receptor-Modified T Cells Recognizing Mesothelin in Advanced Solid Cancers.* Mol Ther, 2019. **27**(11): p. 1919-1929.

28. Watanabe, K., et al., *Pancreatic cancer therapy with combined mesothelin-redirected chimeric antigen receptor T cells and cytokine-armed oncolytic adenoviruses.* JCI Insight, 2018. **3**(7).

29. Kawalekar, O.U., et al., *Distinct Signaling of Coreceptors Regulates Specific Metabolism Pathways and Impacts Memory Development in CAR T Cells.* Immunity, 2016. **44**(2): p. 380-390.

30. Nelson, M.H., et al., *Identification of human CD4(+) T cell populations with distinct antitumor activity.* Sci Adv, 2020. **6**(27).

31. Bailey, S.R., et al., *Human CD26high T cells elicit tumor immunity against multiple malignancies via enhanced migration and persistence.* Nature Communications, 2017. **8**(1).

32. Paulos, C.M., et al., *Adoptive immunotherapy: good habits instilled at youth have long-term benefits.* Immunologic Research, 2008. **42**(1-3): p. 182-196.

33. Kaech, S.M., E.J. Wherry, and R. Ahmed, *Effector and memory T-cell differentiation: implications for vaccine development.* Nature Reviews Immunology, 2002. **2**(4): p. 251-262.

34. Funk, C.R., et al., *PI3Kδ/γ inhibition promotes human CART cell epigenetic and metabolic reprogramming to enhance antitumor cytotoxicity.* Blood, 2022. **139**(4): p. 523-537.

35. Li, Y. and R.J. Kurlander, *Comparison of anti-CD3 and anti-CD28-coated beads with soluble anti-CD3 for expanding human T cells: Differing impact on CD8 T cell phenotype and responsiveness to restimulation.* Journal of Translational Medicine, 2010. **8**(1): p. 104.

36. Carpenito, C., et al., *Control of large, established tumor xenografts with genetically retargeted human T cells containing CD28 and CD137 domains.* Proceedings of the National Academy of Sciences, 2009. **106**(9): p. 3360-3365.

37. Bankhead, P., et al., *QuPath: Open source software for digital pathology image analysis.* Sci Rep, 2017. **7**(1): p. 16878.

38. Sharpless, N.E. and R.A. Depinho, *The mighty mouse: genetically engineered mouse models in cancer drug development.* Nature Reviews Drug Discovery, 2006. **5**(9): p. 741-754.

39. Gerberick, G.F., et al., *Selective Modulation of T Cell Memory Markers CD62L and CD44 on Murine Draining Lymph Node Cells Following Allergen and Irritant Treatment.* Toxicology and Applied Pharmacology, 1997. **146**(1): p. 1-10.

40. Gattinoni, L., et al., *Removal of homeostatic cytokine sinks by lymphodepletion enhances the efficacy of adoptively transferred tumor-specific CD8+ T cells.* Journal of Experimental Medicine, 2005. **202**(7): p. 907-912.

41. Majzner, R.G. and C.L. Mackall, *Tumor Antigen Escape from CAR T-cell Therapy.* Cancer Discovery, 2018. **8**(10): p. 1219-1226.

42. Lohmueller, J.J., et al., *mSA2 affinity-enhanced biotin-binding CAR T cells for universal tumor targeting.* Oncoimmunology, 2017. **7**(1): p. e1368604.

43. Gopinathan, A., et al., *GEMMs as preclinical models for testing pancreatic cancer therapies.* Disease Models & Mechanisms, 2015. **8**(10): p. 1185-1200.

44. Bradney, M.J., et al., *A Biomimetic Tumor Model of Heterogeneous Invasion in Pancreatic Ductal Adenocarcinoma.* Small, 2020. **16**(10): p. 1905500.

45. Imamura, T., et al., *Quantitative analysis of collagen and collagen subtypes I, III, and V in human pancreatic cancer, tumor-associated chronic pancreatitis, and alcoholic chronic pancreatitis.* Pancreas, 1995. **11**(4): p. 357-64.

46. Carstens, J.L., et al., *Spatial computation of intratumoral T cells correlates with survival of patients with pancreatic cancer.* Nature Communications, 2017. **8**(1): p. 15095.

47. Bear, A.S., R.H. Vonderheide, and M.H. O'Hara, *Challenges and Opportunities for Pancreatic Cancer Immunotherapy.* Cancer Cell, 2020. **38**(6): p. 788-802.

48. Du, J., J. Gu, and J. Li, *Mechanisms of drug resistance of pancreatic ductal adenocarcinoma at different levels.* Biosci Rep, 2020. **40**(7).

49. Chen, Y., et al., *Type I collagen deletion in αSMA(+) myofibroblasts augments immune suppression and accelerates progression of pancreatic cancer.* Cancer Cell, 2021. **39**(4): p. 548-565.e6.

50. Miyabayashi, K., H. Ijichi, and M. Fujishiro, *The Role of the Microbiome in Pancreatic Cancer.* Cancers, 2022. **14**(18): p. 4479.

51. Brocker, T., *Chimeric Fv-zeta or Fv-epsilon receptors are not sufficient to induce activation or cytokine production in peripheral T cells.* Blood, 2000. **96**(5): p. 1999-2001.

52. Létourneau, S., et al., *IL-2/anti-IL-2 antibody complexes show strong biological activity by avoiding interaction with IL-2 receptor α subunit CD25.* Proceedings of the National Academy of Sciences, 2010. **107**(5): p. 2171-2176.

53. Majchrzak, K., et al., *β-catenin and PI3Kδ inhibition expands precursor Th17 cells with heightened stemness and antitumor activity.* JCI Insight, 2017. **2**(8).

54. Akce, M., et al., *The Potential of CAR T Cell Therapy in Pancreatic Cancer.* Front Immunol, 2018. **9**: p. 2166.

55. Akhuba, L., Z. Tigai, and D. Shek, *Where Do We Stand with Immunotherapy for Advanced Pancreatic Ductal Adenocarcinoma: A Synopsis of Clinical Outcomes.* Biomedicines, 2022. **10**(12): p. 3196.

56. Liu, Q., et al., *Clinical Strategies for Enhancing the Efficacy of CAR T-Cell Therapy for Hematological Malignancies*, in *Cancers*. 2022, MDPI AG. p. 4452.

57. Ware, B., *Immunization of mice to generate immunological memory responses*. 2022, Chrystal Paulos Lab: IACUC Protocol Records.

APPENDIX I: Protocols

T Cell Harvest Protocol

MATERIALS

1. Mouse spleen (or appropriate PBMCs)
2. EasySep Mouse CD4 T-Cell Isolation Kit + Magnet
    a. StemCell Technologies #19852
3. [CD26 Easy Sep Positive Selection Kit]
4. Dynabeads Mouse T-activator CD3/CD28 Beads
    a. ThermoFisher 11452D
5. Cell strainer (70-micron)
6. RBC Lysis Buffer
7. Culture Media
8. IL2 Aliquot
9. Duvelisib Aliquot
10. PBS

PROCEDURE

Note: This protocol is written for the purposes of plating 100K cells per well in a U-bottom 96-well plate. If more cells are necessary, adjust values accordingly.

Day Zero

Collecting PBMCs

1. Surgically collect mouse spleen, storing in PBS on ice
2. Crush spleen and run through 70-micron cell strainer, rinsing with culture media (CM)
3. Centrifuge at 1100rpm for four minutes
4. Resuspend in 2mL of Red Blood Cell Lysis Buffer for 2 minutes
5. Quench with PBS and centrifuge
6. Resuspend in PBS or Culture Media

If necessary: aliquot sample of cells for Qc negative control

Negative CD4+ T cell Selection (EasySep Protocol)

1. Count cells and resuspend sample at $1*10^{-8}$ cells/mL in recommended media*
    a. *Either Robosep Buffer or PBS with 2% FBS and 1mM EDTA
    b. Final volume should be between 0.25 – 2mL
2. Transfer to polystyrene 5 mL round-bottom tube
3. Add Rat Serum @ 50ul per mL of sample
4. Add Isolation Cocktail @ 50ul per mL of sample
5. Incubate at RT for 10 minutes
6. Vortex RapidSpheres for 30 seconds
7. Add RapidSpheres @ 75ul per mL of sample
8. Incubate at RT for 2.5 minutes
9. Add recommended medium up to 2.5mL total volume, pipette to mix

10. Place tube without lid into magnet and incubate at RT for 2.5 minutes
11. Pick up magnet and pour contents of tube into new container
    a. Do not shake / tap container or drops hanging from mouth of tube
12. Isolated cells are now ready in new container

If Necessary: Aliquot bulk CD4+ Cells here

Positive CD26+ T cell selection (EasySep Protocol)

1. If less than $1*10^7$ cells total: spin and resuspend in 500uL MACs Buffer
    a. If more cells: scale all volumes accordingly
2. Add CD26 antibody at recommended dilution
3. Incubate at room temp for 5 minutes
4. Add 2mL MACS buffer and spin
5. Aspirate and repeat wash step
6. Resuspend in 80uL buffer + 20uL beads
7. Mix and incubate 15 min @ 4C in the dark
8. Add buffer, spin and aspirate
9. Resuspend in 500uL buffer
10. Set up magnetic column with waste tube underneath
11. Run 500uL buffer through column, wait until all of it passes through filter
12. Add sample to column, wait until all of it passes through filter
13. Add 500uL buffer to column x3
14. Place new 15mL tube underneath column **off** magnet
15. Add 1mL buffer to column, promptly push cells through column with plunger
16. Count

CD26+ cells are now ready to use

Plating and Activating Cells for Culture

1. Resuspend cells in culture media @ $1*10^6$ cells / mL
2. Plate 100uL of cells per well
3. Prepare master mix of beads (@ 1:1 w/ cells) and IL-2
    a. $(0.1*10^6$ * # of wells)/ $(40*10^6$ beads/mL) = volume of beads
    b. **WASH Dynabeads prior to use** with PBS or CM
        i. Requires magnet
    c. Mix 490uL CM + 10uL stock IL-2 [10,000IU/mL]
        i. Add 2ul * # of wells of mixed IL-2 to master mix
4. Add 100uL of master mix to each well
5. Create master mix of 300nM duvelisib drug
    a. 2.5uL duvelisib stock [20mM] + 5mL CM
6. Add 6uL of duv. Master mix to each well
    a. Wells WITHOUT duvelisib: add DMSO at same ratio
7. Incubate at 37°C; 5% CO2

Day One: Transduction

1. Transduction protocol located below

Day Two: De-bead and Re-treat

1. Transfer cells and media to Eppendorf tube containing 0.5mL of media

2. Place eppendorf tube on magnet and wait for beads to stick to side **(min. 2 minutes)**
3. Carefully transfer media into new tube without disturbing side with beads
4. Wash beads with 0.5mL of fresh media and repeat magnet process, again transfer media to tube containing cells
5. Spin down cells and resuspend in 200ul of CM
6. Treat with IL-2, Duvelisib, and vehicle control
    a. IL-2: Create MM by combining 10uL stock + 490uL CM, add 2uL per well
        i. NOTE: "Stock" IL-2 = 50,000IU per 10ul aliquot
    b. Duvelisib + vehicle: add using same mixture as day 0
7. Count cells and incubate

NOTE: T cells should be grown for ~~7~~ 5 days before beginning ACT treatment *in vivo*

Mouse T Cell Transduction Protocol

All solutions should be sterile and all steps performed in an aseptic manner in a BSC. Retrovirus must be handled with BSL-2 considerations. See Lab Safety Binder for more information.

Day -7

1. Pull Plat-E cells from cryo, and plate each vial in a T25 flask in 10mL of Plat-E Media.

2. Trypsinize (~1min in incubator) and split cells once confluent (3-4 days). I usually split 1 T25 flask into 2 T175 flasks to keep them in until day 0.

Day 0

1.) Seed 5 million Plat-E* cells in 10mL of DMEM in a 10cm dish, return to incubator at 37°C with 5% CO2

a. Each 10cm dish will yield ~9 mL of virus, which is enough to transduce 3 wells at 2 million T cells per well, so 6 million cells total. Scale up accordingly

Day 1

1.) Transfect the Plat-E cells

a. In one sterile tube mix 0.5mL OptiMEM and 9.3ug of vector DNA. In another sterile tube mix 0.5mL OptiMEM and 18.6uL of Lipofectamine 2000.

b. Add the DNA solution to the Lipofectamine solution. Mix and incubate at room temperature for 5 minutes.

c. Add 1mL of the DNA/Lipofectamine complex slowly, dropwise to the 10cm Plat-E plate. Set plate in the incubator at 32°C with 5.0% CO2.

i. Scale transfection up accordingly

d. After 24 hours in the incubator, carefully remove the transfection media from the plate by pipetting and carefully add 10mL fresh media to the plate. Return to the incubator.

Day 2

1.) After 24 hours in the incubator, carefully remove the transfection media from the plate by pipetting and carefully add 10mL fresh media to the plate. Return to the incubator

2.) Add sodium butyrate to a final concentration of 4mM in the transfection plate. (100 ul of 400 mM stock/plate)

3.) Activate fresh isolated mouse T cells with the appropriate stimulation (i.e. CD3/28 beads, peptide for Pmel/TYRP, etc.)

4.) PM: Coat the # wells needed (1 well=2e6 T cells transduced) of a 24 well non-tissue culture treated plate with 0.5mL of 30ug/mL Retronectin. Wrap with foil and put in 4°C overnight (can also do 2 hrs at RT)

Day 3

NOTE: Day 3 of transduction protocol aligns with day 1 of CD26 Isolation Protocol

1.) Remove retronectin from overnight plate and save in the -20°C for a second use. Block the coated plate with 1mL per well 2% BSA for 30 minutes at room temperature (keep foil on). After blocking, remove, wash 1X with PBS and remove once virus is filtered and ready to use

2.) It takes around 20 min to pre-heat the centrifuge, so start this when you think you have about 20 min left of viral supernatant collection

3.) Meanwhile collect the viral supernatants from the Plat-E plates and filter using a 0.45um PES filter (to remove cells and debris). This can be achieved by using 10 mL pipette. Alternatively, if 2+ dishes of the same virus, collect in a 50mL tube and spin (1100rpm, 4min). and then pour the virus into a new tube and keep on ice until use.

4.) Add 2mL of virus per well of the coated plate and centrifuge at 2000xG for 2 hours at 32°C. Set aside remaining virus on ice.

5.) After the first 2 hour spin is complete, carefully remove the 2mL of viral supernatant from the wells and add 1mL of the T cells (at 2 million/mL) to each well. Then, add 1mL per well of fresh virus that was set aside earlier. Make sure to keep a small aliquot of untransduced cells.

6.) Centrifuge the cells and virus at 1100xg for 2 hours at 32°C. After the spin, collect all of the transduced T cells and re-plate in a new well plate with fresh media/IL-2 (or other cytokines, if necessary). Return to incubator.

Day 4-10

1.) Monitor T cell growth. Refresh media and cytokines or split cells as necessary (usually every other day). Wait at least 24 hours post-transduction to check transduction efficiency by flow (some constructs may take up to 48h to show up by flow).

Media for different cell types:

T cells – complete RPMI (CM)

T2A2 cells – complete RPMI

Phoenix Eco* – DMEM+ 10% FBS

Mel 624 – DMEM+ 10% FBS

Mel 624-28 – DMEM+ 10% FBS

PlatE – DMEM+ 10% FBS, puromycin (1ug/ml), blasticidin (10 ug/ml) (antibiotics in mouse freezer and lab's -20 freezer too)

*Alternative cell line to Plat-E

Preparation of complete RPMI (CM) media for 500 ml total

Add the following components to the 500ml RPMI 1640 (all are found in mouse fridge):

- Fetal calve serum inactivated 50 ml

- 2-Mercaptoethanol 500 ul

- Sodium pyruvate 5 ml

- HEPES 500 ul

- **Glutamine (it may already contain) 5 ml

- Amino acids 5 ml

- Penicillin/streptomycin 5 ml

* How to make 400 mM sodium butyrate:

Dissolve 440.36 mg of sodium butyrate in 10 mL sterile water and filter in hood

* How to make 2% BSA in sterile PBS:

Dissolve 1g BSA (found in big fridge) in 50 mL sterile PBS and filter in hood

Orthotopic Surgery Protocol

Day “Minus” One: the day prior to the orthotopic surgeries

D-1 – Preparation

1. Place frozen matrigel (hallway -20C) on ice in the cold room overnight to thaw.

2. Make surgery packs and autoclave at least one day prior to surgeries.

3. Place syringes, pipette tips, serological pipettes, eppendorfs (1.8mL and 5mL), and 1X PBS, etc. into the -80C so everything is cold for the next morning (prevents matrigel from hardening).

Surgical Pack

-scissors

-suture scissors

-forceps: sharp and less sharp (sutures, finding spleen, tape)

-autoclave tape

-sterile drape

-extra drape to place tool after first mouse

**place in self-seal sterilization pouch (blue plastic) à autoclave (program - GRAV20)

Day Zero:

D0 – Orthotopic Pancreatic Surgeries

keep everything on ice, so the matrigel doesn’t solidify

1. KPC-luc cells prepared for injections: 200,000 cells in 40uL (cold 1x PBS + matrigel)

· Trypsinize (1-2mL) KPC-luc cells and quench trypsin with media (~9-18mL)

· Spin cells down 1500rpm for 5 minutes

· Resuspend cells in COLD 1x PBS and count cells on a hemacytometer

Final Syringe Injection Concentration: need 200,000 KPC-luc cells in 40uL (20uL matrigel + 20uL of cells)

cells + 1x cold PBS concentration = (200,000 cells / 20uL or 107cells / 1mL)

may need to spin cells down again depending on the concentration determined while counting

· Make a 1:1 dilution of the KPC-luc cells (@ 107 cells/mL) with matrigel (i.e. 500uL cells/PBS + 500uL Matrigel) – volumes will depend on how many mice you will be injecting…remember, before making 1:1 dilution consider the following:

due to “dead-space” in the syringe, add ~120-125uL of 1:1 (cells:matrigel) solution into the syringe, so that the syringe has 40uL that will actually get injected into the pancreas – place syringe in ice, now ready for orthotopic injections

technique for adding cells/matrigel to syringe: take out the white/black stopper in the syringe and pipette the matrigel/cell solution on an angle and along the side of the syringe (slowly)

2. Murine Orthotopic Pancreatic Surgeries:

Other materials needed on day of surgery:

Drugs/Equipment (our lab):

-isoflurane (3% gas)

-buprenorphine SR-lab 1mg/kg (pain relief for moderate to severe pain)

-hair clippers

-Nair

-tape for spreading mouse limbs

-ophthalmic eye ointment

Within the DAR mouse facility:

-surgery card (pink)

-clean cage

-outfit: gown, hair cover, gloves, mask

-skin swabs: alcohol (x3) and Prevantics (x3)

-sterile cotton-tipped applicators (for eye prep)

Turn on equipment once in surgery suite:

1. hot bead sterilizer (germinator)

2. water circulating plastic warming pad (white)

3. mouse cage warmer on countertop

4. oxygen concentrator

5. isoflurane vaporizer: tabletop anesthesia unit with isoflurane

-weigh charcoal canisters attached to the induction chamber and nose cone; write on the back of the canister the weight…if canister is 50g à discard (5 gallon bucket) and replace

Sanitize all surfaces before and after use:

1. tabletop and countertop

2. induction chamber: place a paper towel inside the induction chamber

3. appropriate size nose cone (mouse—9mm vs. rat—14mm)

4. cage warmer: wrap the large blue autoclave drape around the warmer: get clean cage—put the mice in after their surgery is over

Paperwork to fill out:

1. Rodent Surgery/Anesthesia Record Log Sheet (pink binder)—above Jackie's desk

2. Controlled substances log for buprenorphine (navy binder)—above Jackie's desk

3. surgical card (pink index card)—located in mouse facility in front of housing room

Surgery:

1. Place cage with mice (for surgery) and clean cage on top the cage warmer.

2. Take mouse and place it in the isoflurane chamber and switch valve, so it flows out; wait until the mouse is asleep.

3. Switch off valve once the mouse is asleep and flush out the induction chamber.

4. Place mouse on its belly (nose in cone) on the white warmer (wrapped in drape) and give put the ophthalmic eye ointment on their eyes and inject buprenorphine.

5. Flip mouse over onto its back (nose in cone) and tape the mouse limbs down.

6. Shave the mouse belly.

7. Add Nair for 30 seconds.

8. Wipe off the hair with 2 alcohol wipes.

9. Use 2 prevantics wipes to wipe down the belly; go in a circular motion from the middle to the outside of the mouse belly. Make sure all hair is removed.

10. ADD THE STERILE DRAPE. TOE PINCH THE MOUSE—make sure it is asleep.

11. Using a scissor, make an incision and cut the skin of the mouse.

12. Make an incision and cut the muscle of the mouse belly.

13. Using the larger forceps go inside the incision and “swipe” from top right to bottom left inside the mouse in order to find spleen and pancreas.

14. Pick up the spleen with the large forceps with your non-dominant hand and inject cells into the head of the pancreas by holding the syringe (cells + matrigel) in your dominant hand.

Goal is for the injection to for a cyst or bubble.

15. Gently place the spleen and pancreas back into the mouse.

16. Suture up the muscle (forward-forward; back-back; forward-forward)àcut with scissor

17. Staple the skin/fur with three staples and place mouse back in cage on the warmer.

Day One, Two, & Three: On the back of the pink surgery card record the activity level of the mouse (#1-4), the date, and your initials at 24, 48, and 72hrs after the surgeries. Take pink surgery card away after 72hrs and staple it to the back of the Aseptic Surgery Log Sheet for the corresponding experiment.

Day Seven: Utilize bioluminescent imaging on day 7 to measure tumor growth and randomize the mice so they can be evenly dispersed throughout various treatment groups.

Single-Cell Clone Isolation, Expansion, and Selection Protocol:

1. Cell transductions were done according to the GeneCopia Protocol
    a. According to Cameron's work optimal **MOI = 10** and optimal puromycin selection concentration ranges from **6.5 – 7.5ug/mL**
    b. Isaac's lab notebook: page 21
    c. Cameron's lab notebook (no. 71): page 83
    d. 24-well groups:
        i. Media Control Wells
        ii. Media + Polybrene Control
        iii. Media + Poly. + lentiviral vector
    e. Transduction Supplies Located in –80 (let's look together)
    f. After transduction, cells were expanded, and aliquots frozen down
2. Puromycin selection occurred over 15 days, starting at 5.5ug/ml and increasing up to 7.5ug/ml
    a. Puromycin selection did not *completely* select for luciferase-expressing cells, hence the following single-cell selections
3. Single-cell expansion protocol:
    a. Dilute population to a concentration of 0.5 cells / 200uL
        i. Serial dilution recommended
    b. Fill 96-well plate with 200ul/well
    c. Grow until wells begin to appear yellow (or cells are detectable)
    d. Expand and transfer individual colonies to 48-well plates and 24-well plates
4. Colonies growing steadily in 24-well plates were tested for luciferase expression
    a. ONE-Glo Luciferase Assay REF: E606A
    b. Viable colonies were re-plated in 6-wells and expanded until sizable stocks were readily available
5. Viable colonies with promising *in vitro* luciferase expression were subcutaneously implanted in mice (n=3 per group) and grown out
    a. Mice were monitored for tumor growth (relative to cell line WT controls) and imaged weekly for luciferase expression
    b. Colonies that (A) grew consistently and (B) expressed luciferase consistently were expanded, frozen down, and moved towards orthotopic validation
6. Five mice orthotopically implanted with either candidate colonies or wildtype cell lines
    a. Monitored same as subcutaneous, with same characteristics being observed
    b. If luciferase expression is stable and increasing, sac mice at predetermined endpoint; weigh tumors and FFPE
    c. NOTE: because transductions will NOT yield luciferase expression as strong as that of KPC-luc, it should be expected that signal will be significantly weaker (auto-exposure can take as long as 2 minutes to capture) and expression may not be detectable for longer periods of time (~10 days)

7. Colonies that have successfully passed orthotopic study should have tumors preserved in FFPE; which should then be stained in comparison to wildtype tumors to validate no phenotype changes have occurred
    a. Markers I used to validate MT5-luc compared to MT5: H&E; Picrosirius Red; CD4; CD8

APPENDIX II: Antibodies for Flow and IHC

CD26+ mesoCAR T Cell Panel

Antibody	Fluorochrome	Dilution	Company Name
Live/Dead	ZombieAqua	1:1000	Biolegend
Unstained Beads	Unstained	0	Biolegend
mesoCAR	AF647	1:500	Jackson ImmunoResearch
CD3	BUV395	1:500	AbCam
CD4	PerCP cy5.5	1:500	AbCam
CD26	PE	1:500	AbCam
Lag3	BV711	1:500	AbCam
Tim3	BV421	1:500	AbCam
CD44	BV 786	1:500	AbCam
CD62L	PE Cy7	1:500	AbCam
PD-1	APC Cy7	1:500	AbCam

TME Infiltration Study Panel

Antibody	Fluorochrome	Dilution	Company	Primary Laser
Live/Dead	Zombie Aqua	1:1000	Biolegend	V7
Unstained	Beads	•	Biolegend	-
Thy1.1	PE cy7	1:500	ThermoFisher	YG9
Thy1.2	BV786		ThermoFisher	V15
mesoCAR	AF647		Jackson ImmunoResearch	R2
CD45	BV570		AbCam	V8
CD3	FITC		AbCam	B2
CD4	APC cy7		AbCam	R7
CD8	V450		AbCam	V3

CD26	PE		AbCam	YG1
Tim3	SB600		AbCam	V10
PD-1	PerCP Cy5.5	""""""	AbCam	B9

IHC Antibodies

Marker	Antibody	Company
Cancer Cells	CK19	AbCam
Hematoxolin & Eosin	n/a	n/a
Helper T Cells	CD4	AbCam
Killer T Cells	CD8	AbCam
Picorsirius Red	n/a	n/a